


Review

# Recent Development in Beta Titanium Alloys for Biomedical Applications

Liang-Yu Chen <sup>1,\*</sup>, Yu-Wei Cui <sup>2</sup> and Lai-Chang Zhang <sup>3,\*</sup> 

<sup>1</sup> School of Materials Science and Engineering, Jiangsu University of Science and Technology, Zhenjiang 212003, China

<sup>2</sup> School of Science, Jiangsu University of Science and Technology, Zhenjiang 212003, China; 18852895250@163.com

<sup>3</sup> School of Engineering, Edith Cowan University, 270 Joondalup Drive, Joondalup, Perth, WA 6027, Australia

\* Correspondence: lychen@just.edu.cn (L.-Y.C.); lc Zhangimr@gmail.com or l.zhang@ecu.edu.au (L.-C.Z.); Tel.: +86-511-844-011-73 (L.-Y.C.); +61-863-042-322 (L.-C.Z.)

Received: 12 July 2020; Accepted: 19 August 2020; Published: 24 August 2020



**Abstract:**  $\beta$ -type titanium (Ti) alloys have attracted a lot of attention as novel biomedical materials in the past decades due to their low elastic moduli and good biocompatibility. This article provides a broad and extensive review of  $\beta$ -type Ti alloys in terms of alloy design, preparation methods, mechanical properties, corrosion behavior, and biocompatibility. After briefly introducing the development of Ti and Ti alloys for biomedical applications, this article reviews the design of  $\beta$ -type Ti alloys from the perspective of the molybdenum equivalency ( $Mo_{eq}$ ) method and  $DV-X\alpha$  molecular orbital method. Based on these methods, a considerable number of  $\beta$ -type Ti alloys are developed. Although  $\beta$ -type Ti alloys have lower elastic moduli compared with other types of Ti alloys, they still possess higher elastic moduli than human bones. Therefore, porous  $\beta$ -type Ti alloys with declined elastic modulus have been developed by some preparation methods, such as powder metallurgy, additive manufacture and so on. As reviewed,  $\beta$ -type Ti alloys have comparable or even better mechanical properties, corrosion behavior, and biocompatibility compared with other types of Ti alloys. Hence,  $\beta$ -type Ti alloys are the more suitable materials used as implant materials. However, there are still some problems with  $\beta$ -type Ti alloys, such as biological inertness. As such, summarizing the findings from the current literature, suggestions for  $\beta$ -type Ti alloys with bioactive coatings are proposed for the future development.

**Keywords:** beta titanium; biomedical implants; porous materials; properties; additive manufacturing

## 1. Introduction

Thanks to their excellent mechanical properties, good corrosion resistance, as well as commendable biocompatibility, titanium (Ti) and its alloys are extensively applied in various fields, especially in the biomedical field [1–6]. According to their microstructures in terms of phase constituents, Ti alloys can be roughly categorized into  $\alpha$ -type Ti alloys, ( $\alpha + \beta$ )-type Ti alloys, and  $\beta$ -type Ti alloys. By comparing other metallic materials for biomedical applications, Ti and Ti alloys have lower density, higher specific strength, and better corrosion resistance than stainless steels and Co–Cr-based alloys [7,8]. For instance, commercially pure titanium (CP–Ti), one of the  $\alpha$ -type Ti alloys, has been used as implant materials for nearly half of a century as the first generation of Ti biomaterials [2,8,9]. Initially, CP–Ti was developed to replace stainless steels and Co–Cr alloys for implants since stainless steels and Co–Cr-based alloys contain unfriendly elements, including Ni, Co, and Cr [2,10]. However, some hard tissues or load-bearing connective tissues have higher requirement of mechanical properties; CP–Ti may not satisfy this requirement due to its moderate strength [11,12]. To get rid of this

limitation,  $\alpha + \beta$ -type Ti alloys were emerged at the right moment and they generally have higher strength than  $\alpha$ -type Ti alloys [2,10,11,13]. Typically, Ti-6Al-4V (in wt.%; the same hereafter unless indicated) is the most frequently employed  $\alpha + \beta$ -type Ti alloy, accounting for 50% of Ti products besides CP-Ti [14]. Nevertheless, Ti-6Al-4V contains toxic V which is harmful to the human body. As such, new dual-phase Ti alloys are developed to replace Ti-6Al-4V, such as Ti-6Al-7Nb and Ti-5Al-2.5Fe [2,10,15–17]. For long-term implantation,  $\alpha + \beta$ -type Ti alloys exhibit good performance owing to their excellent fatigue resistance and good corrosion resistance [18,19]. However, Al is still a questionable element in  $\alpha + \beta$ -type Ti alloys since intaking excessive Al can trigger Alzheimer's disease [20]. In addition, the elastic modulus is another important factor to evaluate the availability of Ti implants. The mismatch elastic moduli between implant and human bone would result in the stress-shielding effect, which is a potential hazard to patients and results in the bone adsorption [2,21]. The elastic modulus of human cortical bone is about 30 GPa, while those of Ti-6Al-7Nb and Ti-6Al-4V are about 110 GPa and 112 GPa [2,18]. Therefore, the moduli of dual-phase Ti alloys are significantly higher than that of the human cortical bone. Things have come a long way since  $\beta$ -type Ti alloys were designed and developed.  $\beta$ -type Ti alloys contain higher amounts of  $\beta$ -stabilizers (such as Mo, Ta, and Zr) and hence have dominant  $\beta$  phase in the microstructure. Due to the non-toxic nature of  $\beta$ -stabilizers,  $\beta$ -type Ti alloys not only have the decreased elastic moduli but also possess improved biocompatibility compared with other types of Ti alloys [22–24]. For instance, the elastic modulus of Ti-24Nb-4Zr-8Sn is about 46–55 GPa [25], which is significantly lower than those of dual-phase Ti alloys. Therefore,  $\beta$ -type Ti alloys have a significantly important position in the biomedical field.

As is known,  $\beta$ -type Ti alloys have been developed in the last three decades. Ti-13Nb-13Zr alloys were firstly applied to the biomedical industry in the 1990s, which have been investigated with respect to the microstructure, phase transformations, and properties for many years [26–32]. Some other  $\beta$ -type Ti alloys were developed in the later years and some techniques and/or approaches were developed some well-known  $\beta$ -type Ti alloys as well, for instance, Ti-15Mo [33–36], Ti-Nb-Ta [37–39], Ti-24Nb-4Zr-8Sn [25,40–44], Ti-35Nb-2Ta-3Zr [45–50], Ti-35Nb-5Ta-7Zr [51–54], Ti-30Nb-4Sn [55,56], Ti-35Nb [57–60], Ti-15Nb-3Mo-3Zr-2Sn [61–64], and so on. However, some raw materials, including Nb, Zr, and Ta, are rare; therefore, the cost of  $\beta$ -type Ti alloys is increased. The high melting points of these materials also lead to the difficulty in the preparation of  $\beta$ -type Ti alloys by traditional technologies [65]. Therefore, low-cost  $\beta$ -type Ti alloys with low-cost alloying elements, such as Cr, Mn, and Fe, are developed recently [66]. As such, many new  $\beta$ -type Ti alloys found their ways into biomedical fields, such as Ti-Mo-Zr-Fe series [67], Ti-15Mo-5Zr-3Al [68], Ti-15Mo-3Nb-3Al [69], Ti-12Mo-5Ta [70], Ti-Fe-Sn series [71], Ti-Fe-Ta series [72,73], Ti-Nb-Fe series [74–76], Ti-Zr-Fe-Cr series [77–79], and so on. Due to their better biocompatibility and low cost, such  $\beta$ -type Ti alloys would be the promising biomedical materials in the future. Therefore, various investigations of  $\beta$ -type Ti alloys have been focusing on improving their properties and tailoring their microstructures. Yang et al. [67] found that the corrosion-wear phenomenon of Ti-12Mo-6Zr-2Fe (TMZF) would be accelerated in the simulated body fluid, which is attributed to the absence of strain hardening. Satendra et al. [80] compared Ti-15Mo with CP-Ti and Ti-6Al-4V alloys by electrochemical measurement in the Ringer's solution and demonstrated that Ti-15Mo alloy has the best corrosion resistance. Afonso et al. [81] investigated the influence of rapid solidification on Ti-xNb-3Fe alloys ( $x = 10, 15, 20, 25, 30$ , and 35 wt.%) and found that the elastic moduli of Ti-xNb-3Fe alloys are related to the microstructure resulted from rapid solidification. Amigó et al. [82] investigated the effects of Fe content (1.5, 3.0, and 4.5 wt.%) on the microstructures and mechanical properties of Ti-35Nb-10Ta-xFe alloys produced by powder metallurgy. The addition of Fe slightly enhanced the stability of alloys but declined the maximum strength and deformability owing to the increased porosity.

Up to date, biomedical  $\beta$ -type Ti alloys have been developed for over thirty years. Therefore, this review aims to give an overall comprehension of biomedical  $\beta$ -type Ti alloys. In this review, an introduction to the development of biomedical Ti and Ti alloys is first presented. As such, the significance of  $\beta$ -type Ti alloys can be understood. Afterward, the alloy design

and processing of  $\beta$ -type Ti alloys are briefly introduced to know how to obtain Ti alloys with a body-centered cubic (BCC) structure at room temperature. With the development of preparation methods, new techniques, such as additively manufacturing, porous powder metallurgy and FAST-forge technology (field-assisted sintering technology, followed by forging), provide brand new ways to produce porous  $\beta$ -type Ti alloys with lower elastic moduli compared with the bulk counterparts. Such techniques shed insight into the preparation of  $\beta$ -type Ti alloys with extremely low moduli. Finally, the properties of  $\beta$ -type Ti alloys, such as the mechanical properties, corrosion behavior, and even biocompatibility, are reviewed in comparison to other types of Ti alloys.

## 2. Design and Processing of Biomedical $\beta$ -type Titanium Alloys

Similar to other hexagonal metals and alloys, Ti exhibits a hexagonal close-packed structure (HCP,  $\alpha$ -Ti) at room temperature and transforms into a BCC  $\beta$ -Ti above the  $\beta$  transus temperature (883 °C for Ti) [22,83–87]. Therefore, to obtain  $\beta$ -type Ti alloys at room temperature, the addition of a relatively high fraction of  $\beta$ -stabilizers, such as Mo, Nb, Ta, Fe, and Cr, is required [46,88,89]. Such  $\beta$ -stabilizing elements expand the  $\beta$  region and form infinite solid solutions with Ti above the  $\beta$  transus temperature in the binary phase diagrams [90,91]. Therefore, generally, Ti alloys would consist of a metastable BCC  $\beta$ -phase after quenching from the temperature above  $\beta$  transus temperature if the addition of  $\beta$ -stabilizers exceeds a critical concentration. For example, a 10 wt.% addition of Mo in Ti–Mo binary alloys can form an infinite solid solution above 400 °C [91]; Ti–Nb binary alloys with 35 wt.% Nb would form an infinite solid solution above 425 °C [90]. However, a metastable BCC  $\beta$ -phase would decompose into an HCP  $\alpha'$ -martensite phase and/or the orthorhombic  $\alpha''$ -martensite in the condition of energy disturbance (including heat treatment and deformation) [72,74]. In such a situation, it is possible to add enough  $\beta$ -stabilizers to lower the  $\beta$  transus temperature below room temperature in principle, thereby resulting in stable  $\beta$ -type Ti alloys.

Usually, the molybdenum equivalency ( $Mo_{eq}$ ) method is used to predict the  $\beta$  phase stability of  $\beta$ -type Ti alloys, which is expressed as the following Equation (1):

$$Mo_{eq} = [Mo] + \frac{[Ta]}{5} + \frac{[Nb]}{3.6} + \frac{[W]}{2.5} + \frac{[V]}{1.5} + 1.25[Cr] + 1.25[Ni] + 1.7[Mn] + 1.7[Co] + 2.5[Fe] - [Al] \quad (1)$$

where  $[x]$  indicates the content of the element  $[x]$  in wt.%. This equation is used to evaluate the equivalent effect of  $\beta$ -stabilizers in Ti alloys. Mo is selected as the baseline and normalizes other elements to an equivalent Mo value. Conversely, Al ( $\alpha$ -stabilizer) plays a subtracted role in the  $Mo_{eq}$  value. Other  $\alpha$ -stabilizers, such as Zr, Sn, O, and N, can also be calculated as Al equivalency ( $Al_{eq}$ ), according to the following equation:

$$Al_{eq} = [Al] + \frac{[Zr]}{5.9} + \frac{[Sn]}{3} + \frac{[O + N]}{0.1} \quad (2)$$

where  $[x]$  also indicates the content of the element  $[x]$  in wt.%. As such, total  $Mo_{eq}$  can be calculated for a variety of Ti alloys. Minor variations may be reported for these two equations, because of the critical concentrations of elements between the American and Russian data [1].

A  $Mo_{eq}$  value of approximately 10.0 is required to obtain 100% BCC  $\beta$ -phase after quenching from the  $\beta$  phase region [91]. The  $\beta$  transus temperature is lowered as the value of  $Mo_{eq}$  increases. The  $Mo_{eq}$  values and  $\beta$  transus temperatures for some commercially  $\beta$ -Ti alloys and newly designed low-cost  $\beta$ -type Ti alloys as well as their elastic moduli are summarized in Table 1. As listed in Table 1, various Ti alloys are designed with different chemical compositions; a higher  $Mo_{eq}$  generally results in more stable  $\beta$ -Ti alloys. The  $Mo_{eq}$  method plays a significant role in designing new  $\beta$ -Ti alloys and has facilitated the development of a wide range of  $\beta$ -Ti alloys in the past decades, such as the Ti–Mo series [92,93], Ti–13Nb–13Zr [30,94], Ti–20Nb–10Zr–5Ta [95], Ti–11.5Mo–6Zr–4.5Sn [96,97], Ti–35Nb–5Ta–7Zr [51,98], and Ti–29Nb–13Ta–4.6Zr [99]. Notably, Mo, Zr, Ta, and Nb metals have

higher density than Ti. Therefore, alloying with such elements would increase the density of Ti alloys. As implants, the increase in weight may cause discomfort for the patients. As mentioned earlier, Mo, Zr, Ta, and Nb are also expensive, and the use of these elements would increase the cost of  $\beta$ -Ti alloys. Moreover, these alloying elements possess high melting points, inevitably causing difficulty in the alloy preparation. As such, new low-cost  $\beta$ -Ti alloys have been developed in recent years based on the molybdenum equivalency method, which primarily contains low-cost alloying elements, such as Fe, Mn, Sn, and Cr [71,72]. Such newly designed low-cost  $\beta$ -Ti alloys also exhibit favorable properties for biomedical applications [100].

**Table 1.** Molybdenum equivalency ( $Mo_{eq}$ ),  $\beta$  transus temperatures, and elastic modulus of some commercially  $\beta$ -Ti alloys and newly designed low-cost  $\beta$ -type Ti alloys.

Alloy	Type	$Mo_{eq}$	Beta Transus (°C)	Elastic Modulus (GPa)	Ref.
Ti-13Nb-13Zr	$\beta$ -rich	1.4	735	79–84	[1,101]
Ti-24Nb-4Zr-8Sn	$\beta$ -rich	1.6	-	46–55	[25]
Ti-33Zr-3Fe-2Cr	Near- $\beta$	4.4	-	138–143	[77]
Ti-20Nb-10Zr-5Ta	Near- $\beta$	5.0	-	59	[102]
Ti-5Al-2Sn-2Cr-4Mo-4Zr-1Fe	Near- $\beta$	5.0	891	-	[1]
Ti-4.5Al-3V-2Mo-2Fe	Near- $\beta$	5.4	900	110	[1,103]
Ti-5Al-2Sn-2Zr-4Mo-4Cr	Near- $\beta$	5.5	884	112	[1,103]
Ti-5Al-5Mo-1Cr-1Fe	Near- $\beta$	8	849	-	[1]
Ti-10V-2Fe-3Al	Near- $\beta$	9.6	805	110	[1,103]
Ti-29Nb-13Ta-4.6Zr	Metastable	10.2	-	80	[2]
Ti-25Nb-8Zr-4Cr	Metastable	10.6	-	50	[79]
Ti-26Nb-4Zr-3Mn	Metastable	11.6	-	32	[104]
Ti-11Nb-3.5Fe	Metastable	11.8	-	101	[76]
Ti-25Nb-3Sn-4Cr	Metastable	11.9	-	75–80	[105]
Ti-11.5Mo-6Zr-4.5Sn	Metastable	12.0	744	83–103	[1,103]
Ti-5V-3Cr-3Sn-3Al	Metastable	12.2	760	-	[1]
Ti-15Mo-2.6Nb-3Al-2Si	Metastable	13.1	806	89	[1,106]
Ti-35Nb-2Ta-3Zr	Metastable	13.9	-	44	[45]
Ti-15Mo	Metastable	14.8	726	78	[1,101]
Ti-12Mo-6Zr-2Fe	Metastable	16.8	-	74–85	[103]
Ti-4.5Fe-6.5Mo-1.5Al	Metastable	18.0	801	-	[1]
Ti-7Fe-11Nb	Metastable	20.5	-	110	[74]
Ti-8Fe-5Ta	Metastable	21.0	-	118–124	[72]
Ti-6V-6Mo-5.7Fe-2.7Al	Metastable	23.8	704	-	[107]
Ti-27Nb-7Fe-2Cr	Metastable	26.8	-	108	[108]

Another important design method is the  $DV-X\alpha$  molecular orbital design method [108]. In this method, two key parameters are used, namely, bond order ( $Bo$ ) and metal d-orbital energy level ( $Md$ ).  $Bo$  indicates the covalent bond strength between metal Ti and an alloying element, and  $Md$  represents the metal d-orbital energy level of transition metals as alloying elements, which is determined by the metallic radius of elements and the electronegativity. Correspondingly, Morinaga et al. established [109–111] the  $\overline{Bo}-\overline{Md}$  diagram to utilize the theoretical approach of the  $d$  electron theory;  $\overline{Bo}$  and  $\overline{Md}$  are average values for  $Bo$  and  $Md$ . This method not only indicates the phase stability and phase constituents of Ti alloy but also can predict their mechanical properties [112]. The  $\overline{Bo}-\overline{Md}$  diagram has been reported in Ref. [101,108,111]. Therefore, many  $\beta$ -type Ti alloys have been developed based on this  $DV-X\alpha$  molecular orbital design method.

According to the aforementioned methods, a variety of  $\beta$ -type Ti alloys were designed and produced in the past [96,113]. Generally,  $\beta$ -type Ti alloys are produced by solidification/casting [93]. Recently, Chirico et al. [114] reported a method to produce  $\beta$ -type Ti alloys using titanium hydride as feedstock by powder metallurgy. Such a method enhances the densification of Ti compacts, gets better control of contamination, and reduces the cost of raw materials. On the other hand,

to obtain a required shape, the produced Ti bulks must undergo thermo-mechanical processing and/or heat treatment, which can also tailor the microstructures of  $\beta$ -type Ti alloys, especially for metastable  $\beta$ -type Ti alloys. As reported in the literature, general thermo-mechanical processing, including forging, rolling, and extrusion, was conducted on  $\beta$ -type Ti alloys to produce rods, sheets, and/or tubes, respectively [113]. In the meantime,  $\beta$ -type Ti alloys are heat treatable and can be heated at solution-treated temperature followed by aging to enhance their strength [1]. The phase transformation of  $\beta \rightarrow \alpha$ ,  $\beta \rightarrow \alpha'$  and/or  $\beta \rightarrow \alpha''$  takes place during aging in the solution-treated metastable  $\beta$ -type Ti alloys, hence causing dispersion strengthening [72]. However, the strength of most  $\beta$ -type Ti alloys have satisfied strength to meet the requirement for use as implants. Therefore, extensive attention has been paid to decrease the elastic moduli of  $\beta$ -type Ti alloys to avoid the stress-shield effect. Although  $\beta$ -type Ti alloys have lower elastic moduli compared with other types of Ti alloys, the elastic moduli of  $\beta$ -type Ti alloys are still higher than those of the human bones. Therefore, porous  $\beta$ -type Ti alloys (other types of Ti and Ti alloys) [41,115–119], in which their strength is sacrificed to obtain lower moduli, are produced by new preparation methods.

### 3. Some Preparation Methods for Porous $\beta$ -type Ti Alloys

As seen in Figure 1, the elastic modulus of human bone is about 30 GPa, while the lowest elastic modulus of Ti–29Ni–13Ta–7.1Zr alloy is 55 GPa. The mismatch of elastic modulus between the implant and adjacent bones would result in the stress-shielding effect [120]. When the stress-shielding effect takes place, the bone would reduce the mass, namely, bone resorption [119,121,122]. It has reported that the stress-shielding effect would lead to the thinning of the bone (external remodeling) or it becoming more porous (internal remodeling) [119,121,122]. Meanwhile, the relative movement between the implant and the adjacent bone would take place owing to the modulus mismatch. Under the extreme situation, bone ingrowth would be inhibited so that implant osseointegration is unsuccessful [119]. Fortunately, the development of porous materials could effectively lower the moduli of Ti and Ti alloys and therefore enable the possibility of the stress-shielding effect. The porous structure not only lowers the elastic moduli of Ti alloys but also enhances tissue adhesion and promotes the ingrowth of bone cells [116,123]. Therefore, it is necessary to develop porous  $\beta$ -type Ti alloys for the actual applications. Up to now, there are a variety of preparation methods for porous materials, such as sintering, investment casting, and rapid prototyping [10,124]. The various preparation methods would lead to the different properties of Ti and Ti alloys. Currently, two primary methods are frequently employed for preparing porous  $\beta$ -type Ti alloys, namely, powder metallurgy and additive manufacturing.

#### 3.1. Powder Metallurgy

Powder metallurgy (PM) uses the powder of pure metals, blends, or alloys as raw materials, and it produces metallic parts by forming and/or sintering [125–130]. Before the process of PM, the powder would be compressed in a mold, which aims to attain the required shapes and dimensions of the model [23,125,131–133]. Afterward, the sintering process is conducted under a protective atmosphere in a high-temperature stove or a vacuum stove. PM allows the fabrication of amorphous materials, solid solutions as well as intermetallic phases from components with different melting points [131,134–136]. In addition, PM technology has high design freedom and could fabricate metallic parts with porous structures on a large scale [10]. The porous metallic parts manufactured by PM may have different types of pores, such as through holes and blind holes [10]. For porous implants, the size and morphology of pores should be controlled in the PM process, which has influences on bone ingrowth, osteointegration, and the fatigue resistance of the implants [137]. PM has been employed to produce Ti and Ti alloys for many years [138]. In recent years, porous Ti alloys are prepared by PM technologies for biomedical applications. Among various PM technologies, spark plasma sintering and the space holder method are commonly used for producing porous Ti and Ti alloys.

Spark plasma sintering (SPS) is a rapid sintering process, which employs the external current to assist powder consolidation [2,10]. SPS directly exerts a pulse current between powder particles for



heating and sintering the powder. Hence, sometimes, SPS is also called plasma-activated sintering, electrical field-activated sintering, or electrical discharge compaction [10]. The SPS device includes a power supply (impulse current generator), pressure control, and vacuum chamber. Before sintering, metal powder is put into a mold and applied with pressing pressure as well as current. Subsequently, the powder used would experience discharge activation, thermoplastic deformation, and cooling. Finally, a high-performance part would be obtained. As such, SPS is a novel technology using electric energy combined with mechanical energy. SPS technology is frequently used in the biomedical field, which results in high biomechanical properties and the osteoconductivity of prepared porous materials [139]. The advantages of low sintering temperature, low electric pressure, and short time make SPS become a priority for porous Ti and its alloys [2]. Hussein et al. [140] successfully prepared nanostructured near- $\beta$  Ti-20Nb-13Zr by SPS, and the results showed that a structure with nearly full density is obtained after SPS at 1200 °C. Sintering at the temperature below 1200 °C can obtain a porous structure (Figure 1a). The obtained alloy was chemically homogenized with a microhardness value ranging from 620 HV to 660 HV (Figure 1b). The developed Ti-20Nb-13Zr alloy prepared by SPS is proposed for dental and/or orthopedic applications.

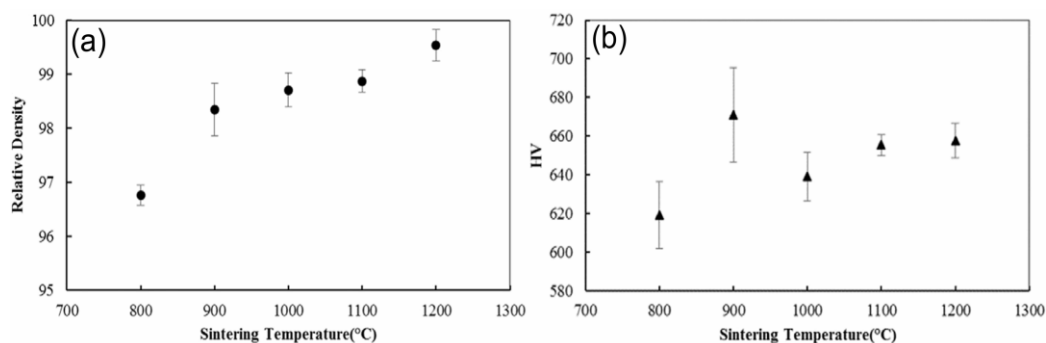


**Figure 1.** Spark plasma-sintered Ti-20Nb-13Zr at different temperatures: (a) relative density and (b) hardness. (Reproduced with permission from ref. [140]. Copyright (2015), Elsevier).

The space holder method is another PM technology, which is a modification of conventional powder metallurgy [141]. The space holder method uses mixed metal powder and spacer particles as raw materials. The spacer particles act as pore formers to assure the homogeneity of the mixture [141,142]. Then, the mixed powder is put into a mold and compressed together under a controlled pressure to form a solid part [10,142–144]. Afterward, either sintering or removal of the spacer (depending on the type of spacer) is used in the process, therefore leaving behind the new pores in the matrix [10,142]. As such, the shape, size, and distribution of the pores, as well as the porosity, all depend on the selected spacer particles [10]. Therefore, it is important to select an appropriate spacer material with low reactivity, which can be removed under relatively low temperatures [2,10]. This method is simple and easy to operate. For example, porous  $\beta$ -type Ti-10Nb-10Zr, with macropores of 300–800  $\mu\text{m}$  and micropores of several microns, is successfully fabricated by this method [145]. The raw powder was primarily mixed with an ammonium hydrogen carbonate spacer. The size of the spacer was about 500–800  $\mu\text{m}$ . Before sintering, the mixture is compressed to compact in a mold. Subsequently, the compact is sintered in two steps: (i) burning out the spacer (175 °C for 2 h) and (ii) sintering the compact (1200 °C for 10 h). According to this procedure, the porous  $\beta$ -type Ti-10Nb-10Zr with different porosity can be produced by adding different fractions of ammonium hydrogen carbonate spacer. By varying the fraction of the spacer, the porosity of produced porous  $\beta$ -type Ti-10Nb-10Zr can be controlled; therefore, the mechanical properties could be manipulated. Porous Ti-35Nb-5Ta-7Zr, Ti-10Mo, and porous Ti-24Nb-4Zr-8Sn (other types of Ti and Ti alloys as well) have also been successfully produced by this method [146,147]. However, it also has some limits to produce porous materials. The accuracy of the pores is low, which may influence the structure of the produced porous material [2].

### 3.2. Additive Manufacturing

Additive manufacturing (AM), namely, 3D printing, is based on the discrete-collecting principle to achieve parts prototyping [148–151]. In contrast to traditional subtractive manufacturing, AM techniques fabricate three-dimensional solid parts by a layer-by-layer method from bottom to top [148,152–154]. There is a range of advantages of AM techniques, including their short production cycle, simple machining process, fast commissioning, and high material utilization rate [155]. More prominently, AM could prepare parts with complex geometry quickly and accurately, which is far more advantageous than the traditional subtractive manufacturing process [152,155–157]. Through years of exploration and practice, AM could be used to produce metallic parts, such as Ti and Ti alloys, using laser or electron beam as heat sources from computer-aided designed (CAD) models [149,158]. In recent years, AM-produced porous Ti alloys attracted a lot of attention; selective laser melting (SLM) and electron beam melting (EBM) stand in the breach in producing high-performance metallic parts [155,159–161].

The SLM device mainly contains a controlling computer system, a laser emitter, a scanning system, and an automatic powder feeder [156]. During the SLM process, metal powder is selectively heated up to complete melting by a computer-controlled laser beam and then quickly solidifies in a protective atmosphere [156]. When the manufacturing of one layer is finished, the build platform would lower by the thickness of a layer. Subsequently, the powder feeding system sends newly applied powder from a moving container and deposits a new layer of powder on the previously formed solid layer [162]. As such, this process is repeated until the entire CAD model is built. As such, SLM is a layer-wise process, which uses a scanning laser beam to selectively melt the metal powder to produce the metallic components with designed geometry (from a CAD model) [156]. In general, the pre-set processing parameter set determines the properties of components. For instance, the relative density is closely related to the laser energy, which is defined as [163]:

$$E = \frac{P}{vts} \quad (3)$$

where  $P$  is the laser power (W),  $v$  is the scan speed ( $\text{mm s}^{-1}$ ),  $t$  is the layer thickness (mm), and  $s$  is scan spacing (mm).  $E$  is a function of these key parameters for the solidification and the quality of SLM-produced  $\beta$ -Ti components, thereby determining their performances. As shown in Figure 2a, Zhang et al. [25] used different laser scanning speeds to fabricate Ti–24Nb–4Zr–8Sn alloy and found that there is a gradual decrease in the density and hardness with increasing scanning speed (Figure 2a). A similar operation on laser energy density would also influence the properties of porous  $\beta$ -type Ti alloys [41,164]. In addition to the processing parameters, the structure of porous  $\beta$ -type Ti alloy is also a main factor influencing their properties. Liu et al. [159] investigated the manufacturing and mechanical behavior of 3 porous structures (cubic, topology optimized, and rhombic dodecahedron) for Ti–24Nb–4Zr–8Sn. As seen from the typical compressive stress–strain curves of these three structures (Figure 2b), the rhombic dodecahedron structure distinctly exhibits lower compressive strength. The cubic structure and topology-optimized structure show similar maximum compressive strengths of 56 MPa and 58 MPa, respectively. The distinctions in the compressive properties of  $\beta$ -type Ti alloys with different structures are attributed to their different energy absorption behaviors in the initial stage of deformation. Regardless of their strength, such porous  $\beta$ -type Ti alloys show significantly low moduli (approaching 1.3–3.3 GPa) compared with the bulk Ti–24Nb–4Zr–8Sn counterparts produced by SLM (53 GPa) [25,159].

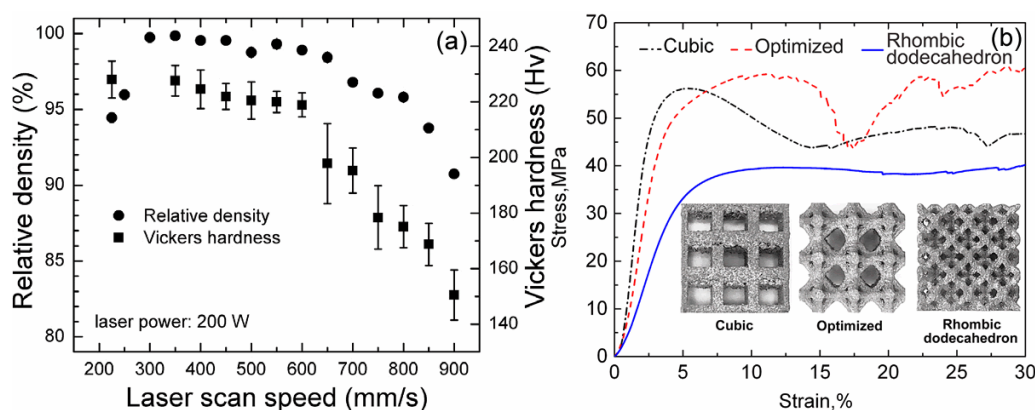


**Figure 2.** (a) Density and Vickers hardness of Ti-24Nb-4Zr-8Sn samples and (b) typical compressive stress–strain curves of Ti-24Nb-4Zr-8Sn alloys with cubic, topology-optimized, and rhombic dodecahedron structures. (Reproduced with permission from refs. [25,159]. Copyright (2011, 2018), Elsevier).

In the early development of SLM technology, only a few Ti alloys were produced due to the lack of pre-alloyed powder, especially the powder from  $\beta$ -type Ti alloys. Therefore, several  $\beta$ -type Ti alloys were produced by mixed powder. Zhao et al. [165] used a Ti-25Nb blend to produce the alloy and found some unmelted Nb particles in the microstructure. Vrancken et al. [166] used Ti-6Al-4V-ELI pre-alloyed powder mixed with 10 wt.% Mo powder to produce a novel metastable  $\beta$  titanium metallic composite and found residual Mo particles in the microstructure. Similar results are also observed for other selective laser melted  $\beta$ -type Ti alloys, such as Ti-35Nb [57], Ti-25Nb [165], Ti-26Nb [167,168], Ti-50Ta [169,170], Ti-37Nb-6Sn [171], Ti-20Zr-12Nb-2Sn [172], etc. The selective laser melted  $\beta$ -type Ti alloys always have heterogeneous microstructures, which has more or less of an influence on their properties. A simple example is the micro-galvanic effect that results from the different phases, which may degrade the corrosion resistance of produced Ti alloys. Therefore, in recent years, more types of pre-alloyed  $\beta$ -type Ti alloy powder have been developed. More  $\beta$ -type Ti alloys produced by selective laser melting were reported, including Ti-45Nb [173], Ti-35Zr-28Nb [174], Ti-15Mo-5Zr-3Al [68], Ti-13Nb-13Zr [175], etc. However, preparing pre-alloyed powder significantly increases the cost of SLM-produced  $\beta$ -type Ti alloys. Therefore, there is a long way to go for the commercial use of SLM-produced  $\beta$ -type Ti alloys.

Similar to SLM, the EBM process, as another AM technique, is capable of fabricating a series of engineering components directly from CAD models using an electron beam as the heat source [152,176,177]. The EBM device generally contains a computer controlling system, a tungsten filament for emitting an electron beam, and a powder feeder system [152]. The electron beam is launched by a tungsten filament when the filament is heated to a certain temperature. During the EBM process, a vacuum environment is used to protect the materials from oxidation. As such, EBM is capable of producing Ti parts with complex geometry directly. The properties of porous  $\beta$ -type Ti alloys are also influenced by the processing parameters of EBM. Liu et al. [42] prepared a porous  $\beta$ -type Ti-24Nb-4Zr-8Sn with 70% porosity using EBM and found that a lower scanning speed results in more input energy; thereby, the produced struts with higher yield strength and fewer flaws. Kurzynowski et al. [178] discussed the effect of the EBM process parameters on the porosity and microstructure of Ti-5Al-5Mo-5V-1Cr-1Fe alloy and pointed out that the maximum hardness is obtained at the energy input of 30 J/mm<sup>3</sup> and the scanning speed of 1800 mm/s. In addition, the Al content in Ti-5Al-5Mo-5V-1Cr-1Fe alloy is related to the scanning speed adopted. The lower the scanning speed (higher energy density), the higher the Al losses. Note that the produced parts of the EBM process have higher environmental (chamber) temperatures compared to the SLM process. The highest preheating temperature of SLM is only 300 °C, while that of EBM could be up to 600–1200 °C [2,42,152]. Hence, the cooling rate in SLM is significantly higher than that in EBM. Such distinctions in the EBM and SLM processes can cause the fabricated parts of  $\beta$ -type Ti alloys produced by EBM and



SLM to have different microstructures and therefore different mechanical properties. Taking  $\beta$ -type Ti–24Nb–4Zr–8Sn (Ti2448) alloy as an example to make a comparison between SLM and EBM, it can be found in Table 2 that the SLM-produced Ti2448 has a slightly higher compressive strength than its EBM-produced counterpart. However, the compressive strength and Young's moduli between SLM- and EBM-produced Ti2448 are almost the same after annealing in the  $\beta$  phase region. These differences are attributed to the production of an  $\alpha$  (or  $\alpha'$ ) phase in Ti2448 during the AM fabrication. Nevertheless, the  $\alpha$  (or  $\alpha'$ ) phase could be dissolved after annealing over 750 °C [115].

**Table 2.** Phase constituents, compressive strength, and Young's modulus of electron beam melting (EBM)- and selective laser melting (SLM)-produced Ti–24Nb–4Zr–8Sn alloy (Ti2448) and human bones.

Material	Method	Phase Constituents	Strength (MPa)	Young's Modulus (GPa)	Ref.
Ti2448 (solid)	SLM	$\beta$	-	$53 \pm 1.00$	[2]
Ti2448 (75% porosity)	SLM	Near- $\beta$	$50 \pm 0.9^c$	$0.95 \pm 0.05$	[115]
Ti2448 (75% porosity)	EBM	Near- $\beta$	$45 \pm 1.1^c$	$1.34 \pm 0.04$	[115]
Ti2448 (75% porosity, annealing)	SLM	$\beta$	$42 \pm 0.5^c$	$1.04 \pm 0.04$	[115]
Ti2448 (75% porosity, annealing)	EBM	$\beta$	$41 \pm 1.1^c$	$1.09 \pm 0.03$	[115]
Tibia (cortical bone)	-	-	$195^t$	28.0	[179]
Femur (cortical bone)	-	-	$194^t$	17.6	[179]
Vertebra (cancellous bones)	-	-	$0.9\text{--}2.5^t$	$0.02\text{--}0.07$	[180]
Lumbar spine (cancellous bones)	-	-	$1.6\text{--}2.5^t$	$0.02\text{--}0.07$	[10]

<sup>t</sup> Ultimate tensile strength; <sup>c</sup> Ultimate compressive strength.

Besides the above most frequently used powder-bed methods, there are also other net-shape fabrication methods to produce porous  $\beta$ -type Ti alloys. For example, laser-engineered net shaping (LENS) involves a complete melting of metal/alloy powder using a high-power laser beam as the heating source to fabricate the net shape (or near-net shape) functional parts [181]. In comparison to SLM and EBM, LENS belongs to the powder-feed method. In the LENS process, a molten metal pool on the substrate is created by a laser. Then, metal/alloy powder is injected into the pool, which melts and solidifies. According to the CAD models used for fabrication, porous structures can be produced. Porous CP–Ti and Ti–6Al–4V have been successfully fabricated by LENS, and their moduli can be tailored by controlling the porosity [119,182,183]. It was reported that the moduli of produced materials can be tailored between 2 and 90 GPa, which well match those of the natural bones [181]. However, due to the lack of  $\beta$ -type Ti alloy, there is rare research with respect to the production of porous  $\beta$ -type Ti alloy. So far, Kalita et al. [184] used the LENS technique to fabricate Ti–14Nb, Ti–17Nb, Ti–19Nb, Ti–23Nb, and Ti–31Nb bulk samples by mixed Ti and Nb powder. Therefore, it is believed that porous  $\beta$ -type Ti alloy may be fabricated by LENS in the near future.

Additionally, there are also some potential methods that can produce porous structures, such as blown powder directed energy deposition [185] and wire fed directed energy deposition [186]. These two methods have successfully fabricated net-shaped Ti parts. Blown powder directed energy deposition has a better capability of producing thin-walled components featuring sharp corners [187] compared with wire fed directed energy deposition. By contrast, wire fed directed energy deposition has a higher deposition rate and lower cost compared to blown powder directed energy deposition [187]. Boeing 787 structural components and external landing gear assembly with complex geometries have been fabricated by wire fed directed energy deposition using Ti–6Al–4V [187]. There still exist rare reports regarding the production of porous  $\beta$ -type Ti alloys by these methods. However, due to the promising capabilities of blown powder directed energy deposition and wire fed directed energy deposition,  $\beta$ -type Ti alloys with complex geometry can also be produced if there is a corresponding feedstock.

### 3.3. FAST-Forge

Apart from additive manufacturing, FAST-forge technology proposed by Weston et al. [188] is another near-net shape fabrication method. This method uses shaped field-assisted sintering to consolidate Ti powder into a pre-forged billet at the first step and then is closed die hot forged to achieve a near-net shape part geometry. The forging step enhances the mechanical properties of the sintered Ti by refining the microstructure. It was reported that Ti–5Al–5V–5Mo–3Cr (Ti–5553, a high-strength  $\beta$ -type Ti alloy) has been successfully prepared by FAST-forge technology. The produced Ti–5553 exhibits a significantly lower grain size of 10  $\mu\text{m}$  compared with its conventionally solution-treated counterpart (approximately 700  $\mu\text{m}$ ) [189]. Therefore, The FAST-forge-produced Ti–5553 has a high hardness between 410 and 417 HV. However, in the authors' opinion, although FAST-forge technology can fabricate Ti parts with the expected geometry, a porous structure with high porosity is still difficult to achieve since the forging process is hardly conducted on the inner Ti part.

## 4. Mechanical Properties

A considerable number of  $\beta$ -type Ti alloys are currently applied as metallic biomaterials as implants, such as artificial hip joints, heart valves, dentistry, and so on [2,190,191]. As such, orthopedic implants would bear the cyclic loading during body movement, which leads to micro-stress concentration by nicks or inhomogeneous microstructures [18]. For a long lifetime of implants, high fatigue resistance and strength are required. In the past, Co–Cr-based alloys and  $\alpha + \beta$ -type Ti alloys are the preferred alloys compared to other biomedical alloys [18]. However, for now,  $\beta$ -type Ti alloys have become the first choice due to their achievable strength and good fatigue resistance [2,18,192]. Kent et al. [193] studied the mechanical properties of Ti–24Nb–3Zr–2Sn–xMo alloys. They found that the cold-rolled Ti–24Nb–3Zr–2Sn–xMo alloys exhibit strength exceeding 900 MPa. Niinomi et al. [194] investigated the Ti–29Nb–13Ta–4.6Zr alloy aging at 573 K and found that the fatigue strength of Ti–29Nb–13Ta–4.6Zr is enhanced while maintaining the modulus below 80 GPa after aging. Therefore, Ti–29Nb–13Ta–4.6Zr could exhibit high fatigue resistance after a suitable thermo-mechanical treatment [18,194,195]. Similarly, Laheurte et al. [196] also had the same conclusion on Ti–29Nb–11Ta–5Zr and Ti–29Nb–6Ta–5Zr.

In addition, an ideal implant material is expected to possess low elastic modulus, good plasticity, and wear resistance besides high fatigue resistance and strength [18,196]. Apparently,  $\beta$ -type Ti alloys demonstrate closer moduli to the human bone in comparison to  $\alpha$ -type Ti alloys and  $\alpha + \beta$ -type Ti alloys. Even if other soft tissues have lower elastic moduli than cortical bones, novel porous structure  $\beta$ -type Ti alloys could satisfy these requirements (Table 2). To obtain the desired mechanical properties of  $\beta$ -type Ti alloys, alloying elements are significantly important. Ehtemam-Haghighi et al. [76] found that the addition of Fe would reduce the formation of  $\alpha''$  martensite and hence improve the stability of the  $\beta$  phase in Ti–11Nb–xFe alloys. With the increasing content of Fe, the strength of Ti–11Nb–xFe also increases. Using such elements to design new  $\beta$ -type Ti alloys with controllable mechanical properties is an available and economic process. Likewise, Jawed et al. [104] found that the addition of Zr and Mn in Ti–Nb alloys would result in different microstructures (Figure 3). Apparently, the microstructures of  $\beta$ -type Ti–Nb–Zr–Mn alloys changes with altering the Zr and Mn contents. The equiaxed  $\beta$  grains are observed in all Ti–Nb–Zr–Mn alloys. It is noted that the addition of Mn reduces the average grain size of Ti–Nb–Zr–Mn alloys. Mn is a high growth-restriction factor when applied to Ti and Ti alloys. During solidification, the addition of Mn results in the rapid buildup of constitutional undercooling, and therefore, nucleation can take place before an advancing solid–liquid interface. Hence, the grains are refined [197]. In comparison, the average grain size of Ti–Nb–Zr–Mn alloys increases with increasing the Zr content. The addition of Zr has both the solution strengthening and fine-grain strengthening effect. Zr also acts as  $\beta$ -stabilizer. When the addition of Zr exceeds a certain content, the stability of the  $\beta$ -phase enhances remarkably, which significantly lowers the  $(\alpha + \beta)/\beta$  phase transformation temperature. As such, the superheat increases markedly and the  $\beta$  grains coarsen [198]. Therefore, the microstructures of Ti–Nb alloys can be tailored. Xu et al. [199] developed a new  $\beta$ -type Ti–5Mo–Fe–3Sn that shows a low elastic modulus of 52 GPa and high yield

strength of 740 MPa. The reason for these desired properties is attributed to the combined addition of Sn and Fe suppressing the formation of the  $\omega$  phase and introducing solid solution strengthening. Hence, selecting the appropriate elements to add to  $\beta$ -type Ti alloys is beneficial to controlling their mechanical properties.

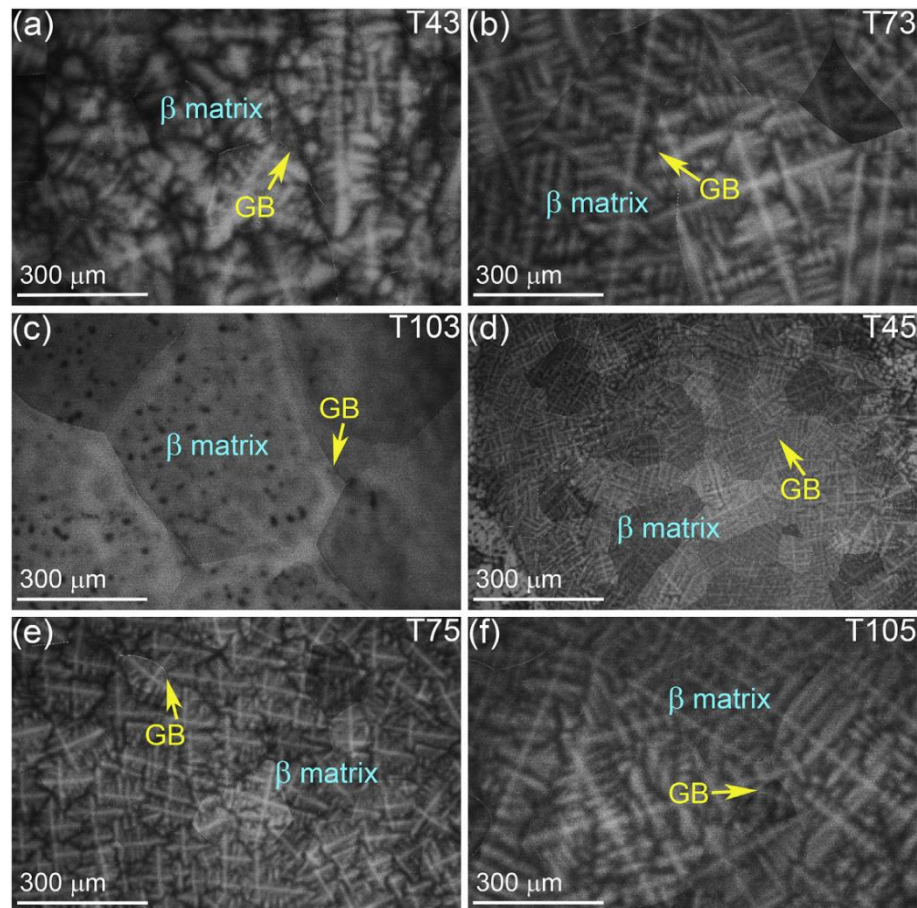


**Figure 3.** Backscattered SEM microstructural features of the Ti-26Nb- $x$ Zr- $y$ Mn (wt.%) alloys: (a) Ti-26Nb-4Zr-3Mn, (b) Ti-26Nb-7Zr-3Mn, (c) Ti-26Nb-10Zr-3Mn, (d) Ti-26Nb-4Zr-5Mn, (e) Ti-26Nb-7Zr-5Mn and (f) Ti-26Nb-10Zr-5Mn. Note that grain boundary is denoted as GB. (Reproduced with permission from ref. [104]. Copyright (2020), Elsevier).

On the other hand, heat treatment and thermo-mechanical processing also can manipulate the microstructures of  $\beta$ -type Ti alloys and tailor their mechanical properties. Liang et al. [200] developed a new  $\beta$ -type Ti alloy of Ti-31Nb-6Zr-5Mo by the  $d$ -electron method using a vacuum nonconsumable furnace. Solution treatment with and without aging treatment were conducted after hot rolling of this alloy. The Nb-rich fibrous grains produced by hot rolling are re-dissolved during solution treatment at 800 °C for 30 min. The alloying elements in Ti-31Nb-6Zr-5Mo become homogeneous after solution treatment. After aging treatment at 300 °C for 2 h, the Nb element redistributes to form the Nb-rich and Nb-depleted  $\beta$  regions. Both solution-treated and aging-treated samples show the identical crystallographic structure of the monolithic  $\beta$  phase. However, different moduli of 44 GPa and 48 GPa are observed for solution-treated and aging-treated samples, respectively. This finding indicates that heat treatment can influence the distribution of alloying elements and therefore the mechanical properties. Coakley et al. [201] found that the cold-rolled Ti-24Nb-4Zr-8Sn exhibits a martensitic  $\alpha''$ -precipitate/ $\beta$ -matrix microstructure. After aging treatment at 300 °C for 4 h and 8 h, the number density of Nb domains (which are associated with superelasticity) decreases, which deteriorates their mechanical properties (Figure 4). Kuroda et al. [202] exerted homogenization, hot rolling,

and annealing on a Ti–20Zr–xMo ternary alloy system (Mo = 0, 2.5, 5, 7.5 and 10 wt.%) and found that the volume fraction of the  $\beta$  phase increases with the increasing Mo content. For homogenized samples, their moduli ranges within 93–105 GPa, regardless of the Mo content. Similar results are also found in the annealed samples [202]. However, for hot-rolled samples, the modulus of the sample decreases with the increasing Mo content. The modulus of Ti–20Zr is  $106 \pm 4$  GPa, which is significantly higher than that of Ti–20Zr–10Mo ( $79 \pm 4$  GPa). This is because hot rolling induces the alteration of the phase constituent of Ti–20Zr–xMo, and the Mo addition increases the stability of the  $\beta$  phase in the microstructure.

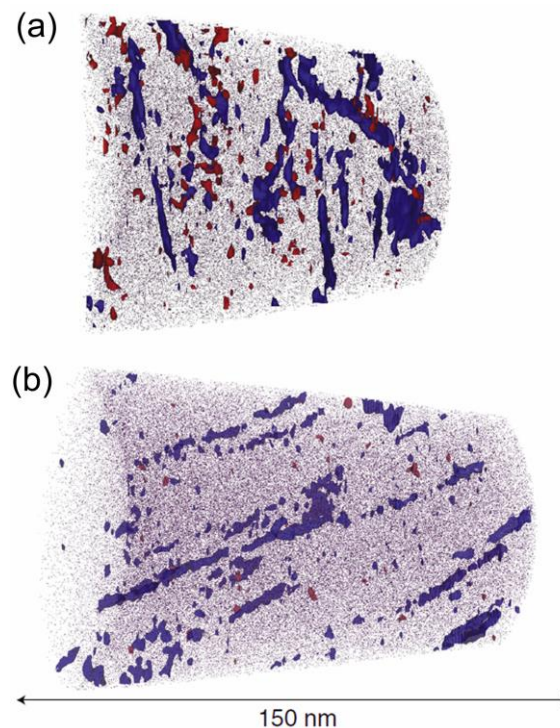


**Figure 4.** Atom-probe tomography reconstructions of Ti 85.5 at.% (blue) and Nb 22.8 at.% (red) for (a) Ti-2448. + 300 °C/4 h, and (b) Ti-2448 + 300 °C/8 h, with 25% of the Zr atoms displayed (purple). It can be found that the number density of Nb domains decreases with the increasing aging time. (Reproduced with permission from ref. [201]. Copyright (2016), Elsevier).

Other microstructural characteristics can also influence the mechanical properties of  $\beta$ -type Ti alloys. Gao et al. [172] pointed out that reducing the grain size of Ti–20Zr–12Nb–2Sn (at.%) would obtain a higher recovery strain, which is an interesting phenomenon. Since the elastic modulus is known to be dependent on the crystallographic orientation of the Ti alloys, controlling their texture can tailor their moduli in theory. For Ti–15Mo–5Zr–3Al alloy, the highest value of the modulus is perpendicular with (111) and the lowest value of the modulus is perpendicular with (001) [203]. Ishimoto et al. [68] used different scan strategies in selective laser melting to control the texture of a Ti–15Mo–5Zr–3Al alloy and successfully obtained a primary (001) texture along with the building direction by a bidirectional scanning strategy with a rotation of 90° between layers (Figure 5). Therefore, a low modulus of Ti–15Mo–5Zr–3Al alloy along with the building direction is achieved. This is because the different scan strategies change the direction of the maximum thermal gradient. Similar work was conducted by Pellizzari et al. [204] using such a method, and they obtained a metastable Ti–15Mo–3Al–3Nb alloy with a low modulus of 53 GPa. Ti–13Nb–13Zr is an early developed metastable  $\beta$ -type Ti alloy with low cost. However, it was reported that the Ti–13Nb–13Zr alloy has a modulus with a lowest boundary of approximately 65 GPa [205]. Lee et al. [205] used cold caliber rolling to process Ti–13Nb–13Zr and



obtained a  $\langle 0002 \rangle$  orientation along with the normal direction. Therefore, a lower modulus of 47 GPa is achieved.

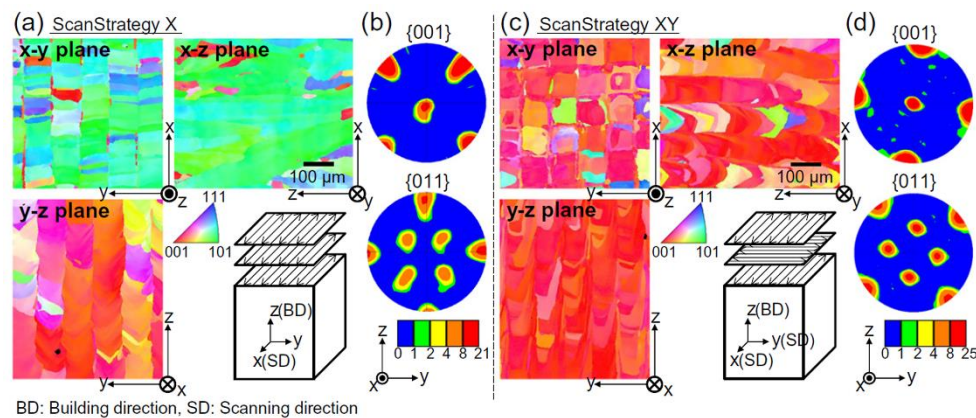


**Figure 5.** (a,c) Inverse pole figure (IPF) images from the three orthogonal planes. (b,d) {001}, and {011} pole figures of the Ti parts measured in the y-z plane. BD is the building direction and SD is the scanning direction. (Reproduced with permission from ref. [68]. Copyright (2017), Elsevier).

Meanwhile, good wear resistance should be considered for  $\beta$ -type Ti alloys also. Yang et al. [67] investigated the corrosion-wear properties of Ti-12Mo-6Zr-2Fe and Ti-6Al-4V in simulated body fluid and found that Ti-12Mo-6Zr-2Fe and Ti-6Al-4V have comparable corrosion-wear resistance, although Ti-12Mo-6Zr-2Fe has a lower hardness. Therefore, Ti-12Mo-6Zr-2Fe can be a candidate for biomedical materials. Table 3 summarizes the mechanical properties of different  $\beta$ -type Ti alloys. Some of the  $\beta$ -type Ti alloys have comparable hardness with  $\alpha + \beta$ -type alloys. The situation is similar in yield strength, while  $\beta$ -type Ti alloys could have higher yield strength than  $\alpha$ -type alloys. The fracture strains of Ti-11Nb-7Fe and Ti-35Nb are significantly higher than that of  $\alpha$ -type Ti alloys. However, the elastic moduli of  $\beta$ -type Ti alloys are significantly lower. Therefore, as the whole, the mechanical properties of  $\beta$ -type Ti alloys are desired.



**Table 3.** Mechanical properties including hardness (H), yield strength ( $\sigma_{0.2}$ ), ultimate strength ( $\sigma_{max}$ ), fracture strain ( $\xi_{max}$ ), and elastic modulus (E) for different types of Ti alloys by a variety of fabrication methods.

Material	Method	Phase Constituents	<i>H</i> (HV)	$\sigma_{0.2}$ (MPa)	$\sigma_{max}$ (MPa)	$\xi_{max}$ (%)	<i>E</i> (GPa)	Ref.
CP-Ti	SLM	$\alpha$	261 ± 13	555	757 <sup>t</sup>	20	106 ± 3	[2]
	Sheet forming		-	280	345 <sup>t</sup>	20	-	
	Fully annealed		-	432	561 <sup>t</sup>	15	-	
Ti-6Al-4V	SLM	$\alpha + \beta$	409	1110	1267 <sup>t</sup>	7	109	[2]
	Casting/superplastic forming		346	847	976 <sup>t</sup>	5	110	
Ti-24Nb-4Zr-8Sn	SLM	$\beta$	220 ± 6	563 ± 38	665 ± 18 <sup>t</sup>	14 ± 4	53 ± 1	[2]
	EBM (70% porosity)	Near- $\beta$	280 ± 5	-	35 ± 2 <sup>c</sup>	-	0.7 ± 0.1	[42]
Ti-11Nb-7Fe	cold crucible levitation	$\beta$	364	985 ± 8	2006 ± 14 <sup>c</sup>	42 ± 2	86 ± 1	[75]
Ti-33Zr-5Fe-4Cr	melting cold crucible levitation	$\beta$	-	1210 ± 10	1711 ± 34 <sup>c</sup>	-	-	[206]
	melting cold crucible levitation							
Ti-27Nb-7Fe-8Cr	melting cold crucible levitation	$\beta$	345	940 ± 23	2000 <sup>c</sup>	-	72 ± 5	[108]
Ti-25Nb-5Sn-4Cr	melting cold crucible levitation	$\beta$	208	411 ± 13	5090 <sup>c</sup>	-	-	[105]
	melting cold crucible levitation							
Ti-25Nb-3Zr-3Mo-2Sn	SLM	$\beta$	202	592 ± 21	716 ± 14 <sup>t</sup>	-	-	[61]
	Hot-rolled		223~230	308 ± 13	622 ± 21 <sup>t</sup>	-	-	
Ti-26Nb-5Mn-10Zr	cold crucible levitation	$\beta$	228 ± 4	488 ± 19	1900 <sup>c</sup>	-	-	[104]
	melting cold crucible levitation							
Ti-33Zr-7Fe-2Cr	melting cold crucible levitation	$\beta$	416	1285 ± 42	1566 ± 49 <sup>t</sup>	-	-	[207]
Ti-12Mo-6Zr-2Fe	-	$\beta$	300 ± 8	911 ± 23	927 ± 8 <sup>t</sup>	-	82 ± 6	[67]
Ti-35Nb	SLM	$\beta$	-	660 ± 13	-	47 ± 1	85 ± 1	[57]

<sup>t</sup> Ultimate tensile strength; <sup>c</sup> Ultimate compressive strength.

## 5. Corrosion Behavior

It is well known that Ti and its alloys demonstrate good corrosion resistance in the various environments due to the formation of a stable passive film (mainly consisting of  $\text{TiO}_2$ ) [2,158,208–210]. Even if the passive film on Ti samples is broken, the passive film can be re-built in a very short time. In the early stage,  $\alpha$ -type and  $\alpha + \beta$ -type Ti alloys are commonly applied for biomedical applications. Generally, the corrosion behavior of metallic materials depends on several factors: applied environment, alloy compositions, and microstructure [127,211–214]. The human body has a relatively stable environment, while human temperature, environmental chemistry, and pH would change in some cases (e.g., inflammation and allergy). Alves et al. [215] investigated the corrosion resistance of CP-Ti and Ti-6Al-4V in simulated body fluid at 25 °C and 37 °C, respectively and found that the corrosion resistance of CP-Ti and Ti-6Al-4V is better at 25 °C. Therefore, the temperature has a significant influence on the corrosion behavior of CP-Ti and Ti-6Al-4V. Similarly, the pH value also influences the corrosion behavior of Ti-6Al-4V [216]. In the neutral Ringer's solution, Ti-6Al-4V has good corrosion resistance, while its passive range is reduced at pH = 8 [216]. According to the literature [217], Ti-6Al-4V exhibits duct-shaped pits along the grain boundaries in the simulated body fluid, which is considered to be related to the dissolution of V-rich zones. As such, the pitting corrosion of Ti-6Al-4V often takes place in the oral environment, which is attributed to the greater availability of oxygen and acidic foods [3]. Kumar et al. [80] found that Ti-15Mo, CP-Ti, and Ti-6Al-4V alloys all have good corrosion resistance in Ringer's solution, while only Ti-15Mo shows a stable passive film in the fluoride solution. The high fluoride solution is inevitable in the human body environment, such as dental cleaning [209,217]. Therefore,  $\alpha$ -type and  $\alpha + \beta$ -type Ti alloys show inferior corrosion resistance compared with  $\beta$ -type Ti alloys in such environments. Furthermore, for bearing metallic orthopedic implants, fretting corrosion should be considered [217]. Fretting corrosion is usually presented at modular junctions and decreases via the formation of a protective oxide layer [217]. Hence, it is highly essential to select appropriate Ti alloys with high corrosion resistance for biomedical applications.

Thanks to the development of  $\beta$ -type Ti alloys, they become candidates for biomedical applications. It is reported that  $\beta$ -type Ti alloys have good performance in a variety of corrosive environments. Wang et al. [57] found that an SLM-produced Ti-35Nb alloy could quickly form a stable passive film (mainly consisting of  $\text{TiO}_2$  and  $\text{Nb}_2\text{O}_5$ ) to protect itself. The stable passive film covers the entire metal surface and effectively reduces the corrosion rate. However, the quality of the passive film is significantly influenced by the chemical homogeneity of the underlying substrate. Generally, SLM-produced Ti-35Nb using mixed powder always results in a heterogeneous microstructure with individual Nb grains. Wang et al. [57] found that the heat treatment of SLM-produced Ti-35Nb at 1000 °C for 24 h in an Ar atmosphere significantly promotes the chemical homogeneity of the Ti-35Nb substrate. Therefore, the heat-treated Ti-35Nb has a higher corrosion potential of  $-0.46$  V versus saturated calomel electrode (SCE) than the SLM-produced Ti-35Nb ( $-0.55$  V versus SCE). Alves et al. [211] also demonstrated that the corrosion resistance of  $\beta$ -type Ti alloys depends on the stability of passive films. They found that Ti-10Mo alloy shows significantly low passive current densities, especially after heat treatment. Certainly, there are many comparative investigations with respect to the corrosion behavior of three types of Ti alloys, which aim to develop more appropriate Ti alloys for biomedical applications. Bai et al. [43] compared the corrosion behavior among CP-Ti, Ti-6Al-4V, and Ti-24Nb-4Zr-8Sn in the simulated physiological environment. Their results showed that the Ti-24Nb-4Zr-8Sn alloy has a wider passive region as compared to CP-Ti and Ti-6Al-4V. Moreover, the Ti-24Nb-4Zr-8Sn alloy has a relatively low corrosion current density, which is comparable to CP-Ti and Ti-6Al-4V, attributing to the formation of the stable passive film primarily consisting of titanium and niobium oxides on its surface. Kumar et al. [80] also studied the corrosion behavior of CP-Ti, Ti-6Al-4V, and Ti-15Mo in the Ringer's solution, and they found that the passivation range of Ti-15Mo alloy (166–2513 mV versus SCE) is greater than those of CP-Ti (145–1522 mV versus SCE) and Ti-6Al-4V (155–1460 mV versus SCE). Chui et al. [218] investigated the corrosion behavior of the as-cast Ti-Zr-Nb-Mo alloys with different Mo contents. The results showed that the grain size of the Ti-Zr-Nb-Mo alloy decreases with increasing

Mo content due to the presence of Mo causing constitutional undercooling, and the Ti–Zr–Nb–Mo alloy with a 15 wt.% addition of Mo shows the lowest passivation current density of  $2.31 \pm 0.03 \mu\text{A cm}^{-2}$ . Zareidoost et al. [219] separately added Fe, Sn, and Ag to Ti–25Zr–10Nb–10Ta and found that the alloy with Ag addition shows the best corrosion resistance in the Ringer’s solution. The standard electrode potential of Ag (0.799 V) is more positive than that of Ti (−0.98 V), leading to the increase in the stability of passive film formed on Ti–25Zr–10Nb–10Ta. Therefore, Ti–25Zr–10Nb–10Ta–1.5Ag shows better corrosion resistance in Ringer’s solution. Lin et al. [220] controlled the microstructure of Ti–40Ta–22Hf–11.7Zr by different solution treatment and aging treatment schemes. The results showed that the as-cast Ti–40Ta–22Hf–11.7Zr shows a  $\beta + \omega$  microstructure, which transforms to monolithic  $\beta$  phase after being solution-treated at 900 °C for 1 h. After aging at 300 °C for 15 min, 1.5 h, 12 h, and 24 h, the  $\beta$ -phase gradually transforms into  $\beta + \alpha''$ ,  $\beta + \alpha'' + \alpha$ , and  $\beta + \alpha + \omega$ . Such different microstructures of Ti–40Ta–22Hf–11.7Zr alloys cause their distinct electrochemical behavior in Hank’s solution. The solution-treated sample with a single  $\beta$  microstructure shows the lowest current density of  $0.49 \pm 0.03 \mu\text{A cm}^{-2}$ .

In several previous studies, the SLM-produced Ti–6Al–4V alloys would be prone to pitting corrosion in 3.5 wt.% NaCl solution compared with the counterparts produced by traditional methods, while EBM-produced Ti–6Al–4V alloy has better corrosion resistance than the wrought counterpart in phosphate-buffered saline [158,221]. Therefore, an open question is asked: Is there a distinct corrosion behavior of Ti alloys produced by different preparation methods? To answer this question, Qin et al. [157] compared the corrosion behavior of SLM-produced and traditional monolithic Ti–24Nb–4Zr–8Sn alloys. These two alloys have the same chemical composition and monolithic  $\beta$  phase but different microstructures. As seen from Figure 6 [157], the potentiodynamic polarization curves and Nyquist plots of both alloys are nearly overlapping. Therefore, it can be understood that the distinctions in the corrosion behavior of Ti–6Al–4V alloys produced by different methods are related to the formation of different phase constituents in the microstructure. In comparison, monolithic  $\beta$ -phase Ti–24Nb–4Zr–8Sn alloys produced by various methods show similar corrosion behavior. Meanwhile, due to their monolithic phase in the microstructure, many  $\beta$ -type Ti alloys also possess high pitting corrosion resistance. However, for some metastable  $\beta$ -type Ti alloys, thermo-mechanical processing and heat treatment may trigger the phase transformation of  $\beta \rightarrow \alpha$ ,  $\beta \rightarrow \alpha'$ , and/or  $\beta \rightarrow \alpha''$ . Therefore, different phases in the microstructure of Ti alloys would produce the micro-galvanic effect during corrosion [222]. Table 4 lists the corrosion potentials, corrosion current densities, and high-potential passive current densities of Ti–6Al–4V ELI, Ti–35Nb–7Zr–5Ta, Ti–13Mo–7Zr–3Fe (as-received  $\alpha + \beta$ ), and Ti–13Mo–7Zr–3Fe (metastable  $\beta$ ) alloys in Ringer’s solution at 37 °C after 1-h immersion [222]. Both Ti–13Mo–7Zr–3Fe (as-received  $\alpha + \beta$ ) and Ti–13Mo–7Zr–3Fe (metastable  $\beta$ ) alloys show better corrosion resistance than Ti–6Al–4V, and monolithic-phase Ti–13Mo–7Zr–3Fe (metastable  $\beta$ ) exhibits better corrosion resistance than Ti–13Mo–7Zr–3Fe (as-received  $\alpha + \beta$ ). Therefore, it can be understood that the corrosion behavior of Ti alloys is mainly influenced by their phase constituents.

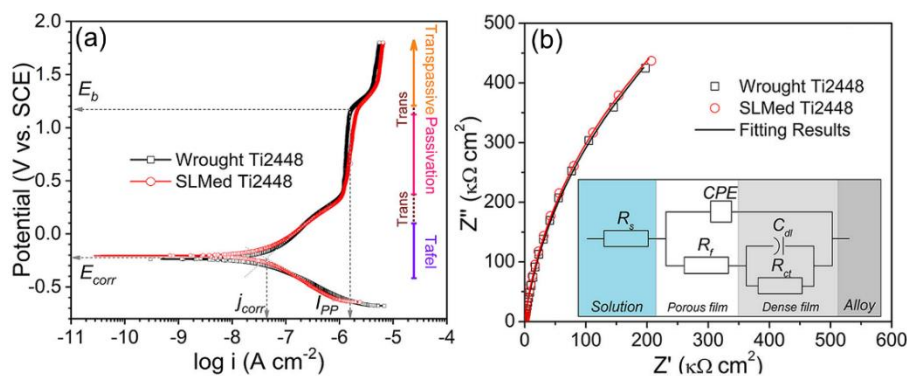


**Figure 6.** Electrochemical measurements of selective laser melted and wrought Ti-24Nb-4Zr-8Sn: (a) Potentiodynamic polarization curves and (b) Nyquist plots (the inset is the equivalent circuit diagram). Ti2448 indicated Ti-24Nb-4Zr-8Sn. (Reproduced with permission from [157]. Copyright (2019), ACS Publications).

**Table 4.** Corrosion potentials, corrosion current densities, and high-potential passive current densities of the Ti-6Al-4V ELI, Ti-35Nb-7Zr-5Ta, Ti-13Mo-7Zr-3Fe (as-received  $\alpha + \beta$ ), and Ti-13Mo-7Zr-3Fe (metastable  $\beta$ ) alloys in Ringer's solution at 37 °C after 1-h immersion [222].

Material	Corrosion Potential (mV vs. SCE)	Corrosion Current Density ( $\mu\text{A cm}^{-2}$ )	Passivation Current Density ( $\mu\text{A cm}^{-2}$ )
Ti-13Mo-7Zr-3Fe ( $\alpha + \beta$ )	$-421 \pm 12$	$29 \pm 15$	$2.2 \pm 0.1$
Ti-13Mo-7Zr-3Fe ( $\beta$ )	$-343 \pm 83$	$20 \pm 10$	$2.1 \pm 0.1$
Ti-35Nb-7Zr-5Ta	$-292 \pm 6$	$12 \pm 5$	$1.9 \pm 0.4$
Ti-6Al-4V ELI	$-380 \pm 65$	$31 \pm 13$	$2.9 \pm 0.4$

Generally,  $\text{Cl}^-$  is presented in a variety of environments, such as the human body, marine, coast environment, and chemical environment [223–225].  $\text{Cl}^-$  ions are aggressive ions in the corrosive environments, which can damage the passive film formed on many metallic components [226–228]. Therefore, the investigation on the corrosion behavior of Ti alloys in the  $\text{Cl}^-$  environment can estimate their corrosion rates. Schutz [229] summarized the corrosion rate of various Ti alloys in boiling HCl solution at different concentrations and pointed out that most  $\beta$ -type Ti alloys show better corrosion resistance than Ti-6Al-4V. This finding illustrates that the passive films formed on  $\beta$ -type Ti alloys are more stable than that formed on Ti-6Al-4V. The better corrosion resistance enables  $\beta$ -type Ti alloys to be good potential biomedical materials.

## 6. Biocompatibility

Apart from the mechanical and corrosion properties, excellent biocompatibility is required for implant materials. Ideal materials can be implanted in the human body for a long period without a second surgery. After implantation, the materials would induce a considerable number of reactions in the human body with body fluid, proteins, and cells. Conventional  $\alpha + \beta$ -type Ti alloys always contain detrimental elements. Therefore,  $\beta$ -type Ti alloys have been developed in recent years, and the corresponding investigation on the biocompatibility of  $\beta$ -type Ti alloys was also conducted. McMahon et al. [230] compared the cytocompatibility between Ti-26Nb and Ni-49.2Ti, and they found that Ti-26Nb is less cytotoxic. Xue et al. [231] pointed out that the Ti-19Zr-10Nb-1Fe alloy has similar cytocompatibility with the Ni-Ti alloy but better hemocompatibility. The improved biocompatibility of  $\beta$ -type Ti alloys can be attributed to the absence of toxic alloying elements. Up to date, the investigation on the biocompatibility of  $\beta$ -type Ti alloys is still at a very early stage. Further investigation regarding  $\beta$ -type Ti alloys is imminent required.

On the other hand, due to the biological inertia of Ti alloys, fibrous tissue capsules are prone to form on the implant surface [2]. Such a phenomenon is inevitable for all types of Ti alloys. The biological

inertness leads the  $\beta$ -type Ti alloys to be safe but not bioactive. Therefore, although  $\beta$ -type Ti alloys are free of toxic alloying elements, further improving the capability of osseointegration should be considered. Generally, surface modification with the aim to improve the bioactivity of Ti alloys has received a considerable amount of attention. For such a purpose, Takematsu et al. [232] conducted alkali solution treatments on Ti-29Nb-13Ta-4.6Zr by electrochemical, hydrothermal, or mixed processes for different times, and the results showed that regardless of the methods or parameters used, the surface of Ti-29Nb-13Ta-4.6Zr becomes mesh-like and has a strong ability to induce the formation of apatite. Dikici et al. [233] synthesized calcium phosphate/TiO<sub>2</sub> composite coatings on Ti-29Nb-13Ta-4.6Zr by the sol-gel method; they found that the coating can significantly enhance its bioactivity, since both calcium phosphate and TiO<sub>2</sub> are highly bioactive to bone cells. Besides inorganic coatings, organic coatings (or layers) have also received extensive attention. In the last few decades, the immobilization of extracellular matrix (ECM) proteins on the surface of Ti implants has been developed, which has been conducted on CP-Ti and Ti-6Al-4V [234]. For instance, CP-Ti coated with collagen has a higher bioactivity for human mesenchymal cells [234]. Similar results are also found in other coatings [235]. Unfortunately, there is still rare literature about the organic coatings on  $\beta$ -type Ti alloys. However, due to the large success of organic coatings on other types of Ti alloys,  $\beta$ -type Ti alloys with bioactive coatings are expected to be a future trend for biomedical Ti alloys.

## 7. Conclusions

Good mechanical properties, excellent corrosion resistance, and admirable biocompatibility are the basic requirements for biomedical materials. Therefore,  $\beta$ -type Ti alloys are the preferred choice. As such,  $\beta$ -type Ti alloys have received a considerable amount of attention in the past few decades. For better development and application in the future, many studies have been conducted to investigate the  $\beta$ -type Ti alloys from alloy design and manufacture to properties. Therefore, this review introduces the biomedical  $\beta$ -type Ti alloys in terms of development, design, new preparation methods, and various properties. Biomedical  $\beta$ -type Ti alloys are developed later than  $\alpha$ -type and  $\alpha + \beta$ -type Ti alloys in the requirements of low elastic modulus and non-toxic alloying elements. Designing a  $\beta$ -type Ti alloy requires the addition of a certain fraction of  $\beta$ -stabilizers. The molybdenum equivalency ( $Mo_{eq}$ ) method is frequently used to predict the  $\beta$ -phase stability of  $\beta$ -type Ti alloy, which is also considered as a significant convenience for designing new  $\beta$ -type Ti alloys. Although  $\beta$ -type Ti alloys have lower elastic moduli than other types of Ti alloys, the elastic moduli of  $\beta$ -type Ti alloys are still higher than those of human bones. Therefore, porous  $\beta$ -type Ti alloys with lower elastic modulus as well as higher tissue adhesion are developed. Additive manufacture (such as selective laser melting and electron beam melting) and powder metallurgy (such as spark plasma sintering and the spacer hold method) are commonly used to produce porous  $\beta$ -type Ti alloys. Afterwards, the properties of  $\beta$ -type Ti alloys are reviewed in view of their mechanical properties, corrosion behavior, and biocompatibility. Fortunately,  $\beta$ -type Ti alloys could perform well in these three aspects. Although  $\beta$ -type Ti alloys have been used as biomedical materials, further investigations are still recommended to increase their reliability and bioactivity in the human body in long-term service. Therefore, in the authors' opinion, porous  $\beta$ -Ti alloys with bioactive coatings may be the future trend for biomedical implants.

**Author Contributions:** Conceptualization: L.-Y.C., Y.-W.C. and L.-C.Z.; writing—original draft preparation: L.-Y.C. and Y.-W.C.; writing—review and editing: L.-Y.C. and L.-C.Z.; writing—manuscript finalization: L.-Y.C. and L.-C.Z.; supervision: L.-C.Z.; project administration: L.-Y.C. and L.-C.Z.; funding acquisition: L.-Y.C. and L.-C.Z. All authors have read and agreed to the published version of the manuscript.

**Funding:** The authors would like to acknowledge the financial support provided by Jiangsu Province six talent peaks project (XCL-117), the Australian Research Council Discovery Project (DP110101653), Open Foundation of Guangxi Key Laboratory of Processing for Non-ferrous Metals and Featured Materials, Guangxi University (Grant No. 2020GXYSOF01, 2019GXYSOF01), Key Research and Development Program of Shaanxi (Program No.2020GY-251).

**Acknowledgments:** The authors are grateful to Liqiang Wang and Qin Peng.

**Conflicts of Interest:** The authors declare no conflict of interest.



## References

1. Kolli, R.P.; Devaraj, A. A review of metastable beta titanium alloys. *Metals* **2018**, *8*, 506. [\[CrossRef\]](#)
2. Zhang, L.C.; Chen, L.Y. A review on biomedical titanium alloys: Recent progress and prospect. *Adv. Eng. Mater.* **2019**, *21*, 1801215. [\[CrossRef\]](#)
3. Geetha, M.; Singh, A.K.; Asokamani, R.; Gogia, A.K. Ti based biomaterials, the ultimate choice for orthopaedic implants—A review. *Prog. Mater. Sci.* **2009**, *54*, 397–425. [\[CrossRef\]](#)
4. Wang, L.; Xie, L.; Zhang, L.-C.; Chen, L.; Ding, Z.; Lv, Y.; Zhang, W.; Lu, W.; Zhang, D. Microstructure evolution and superelasticity of layer-like NiTiNb porous metal prepared by eutectic reaction. *Acta Mater.* **2018**, *143*, 214–226. [\[CrossRef\]](#)
5. Wang, L.; Wang, C.; Zhang, L.-C.; Chen, L.; Lu, W.; Zhang, D. Phase transformation and deformation behavior of NiTi-Nb eutectic joined NiTi wires. *Sci. Rep.* **2016**, *6*, 23905. [\[CrossRef\]](#)
6. Zhang, L.C.; Shen, Z.Q.; Xu, J. Glass formation in a (Ti, Zr, Hf)–(Cu, Ni, Ag)–Al high-order alloy system by mechanical alloying. *J. Mater. Res.* **2003**, *18*, 2141–2149. [\[CrossRef\]](#)
7. Okazaki, Y.; Gotoh, E. Comparison of metal release from various metallic biomaterials in vitro. *Biomaterials* **2005**, *26*, 11–21. [\[CrossRef\]](#)
8. Niinomi, M.; Nakai, M.; Hieda, J. Development of new metallic alloys for biomedical applications. *Acta Biomater.* **2012**, *8*, 3888–3903. [\[CrossRef\]](#)
9. Niinomi, M. Recent metallic materials for biomedical applications. *Metall. Mater. Trans. A* **2002**, *33*, 477–486. [\[CrossRef\]](#)
10. Li, Y.; Yang, C.; Zhao, H.; Qu, S.; Li, X.; Li, Y. New developments of Ti-based alloys for biomedical applications. *Materials* **2014**, *7*, 1709–1800. [\[CrossRef\]](#)
11. Marc, L.; Rack, H.J. Titanium alloys in total joint replacement—A materials science perspective. *Biomaterials* **1998**, *19*, 1621–1639.
12. Ataee, A.; Li, Y.; Wen, C. A comparative study on the nanoindentation behavior, wear resistance and in vitro biocompatibility of SLM manufactured CP-Ti and EBM manufactured Ti64 gyroid scaffolds. *Acta Biomater.* **2019**, *97*, 587–596. [\[CrossRef\]](#) [\[PubMed\]](#)
13. Guo, S.; Shi, Y.; Liu, G.; Wu, R.; Luo, R.; Peng, C.-T.; Meng, Q.; Cheng, X.; Zhao, X. Design and fabrication of a ( $\beta + \alpha''$ ) dual-phase Ti-Nb-Sn alloy with linear deformation behavior for biomedical applications. *J. Alloys Compd.* **2019**, *805*, 517–521. [\[CrossRef\]](#)
14. Wen, Y.; Xie, L.; Wang, Z.; Wang, L.; Lu, W.; Zhang, L.-C. Nanoindentation characterization on local plastic response of Ti-6Al-4V under high-load spherical indentation. *J. Mater. Res. Technol.* **2019**, *8*, 3434–3442. [\[CrossRef\]](#)
15. Polozov, I.; Sufiiarov, V.; Popovich, A.; Masaylo, D.; Grigoriev, A. Synthesis of Ti-5Al, Ti-6Al-7Nb, and Ti-22Al-25Nb alloys from elemental powders using powder-bed fusion additive manufacturing. *J. Alloys Compd.* **2018**, *763*, 436–445. [\[CrossRef\]](#)
16. Semlitsch, M.F.; Weber, H.; Streicher, R.M.; Schön, R. Joint replacement components made of hot-forged and surface-treated Ti-6Al-7Nb alloy. *Biomaterials* **1992**, *13*, 781–788. [\[CrossRef\]](#)
17. Ninomi, M.; Gong, B.; Kobayashi, T.; Ohyabu, T.; Toriyama, O. Fracture characteristics of Ti-6Al-4V and Ti-5Al-2.5 Fe with refined microstructure using hydrogen. *Met. Mater. Trans. A* **1995**, *26*, 1141–1151. [\[CrossRef\]](#)
18. Abdel-Hady Gepreel, M.; Niinomi, M. Biocompatibility of Ti-alloys for long-term implantation. *J. Mech. Behav. Biomed. Mater.* **2013**, *20*, 407–415. [\[CrossRef\]](#)
19. Zhao, S.; Li, S.J.; Wang, S.G.; Hou, W.T.; Li, Y.; Zhang, L.C.; Hao, Y.L.; Yang, R.; Misra, R.D.K.; Murr, L.E. Compressive and fatigue behavior of functionally graded Ti-6Al-4V meshes fabricated by electron beam melting. *Acta Mater.* **2018**, *150*, 1–15. [\[CrossRef\]](#)
20. Azadbakht, R.; Almasi, T.; Keypour, H.; Rezaeivala, M. A new asymmetric Schiff base system as fluorescent chemosensor for Al<sup>3+</sup> ion. *Inorg. Chem. Commun.* **2013**, *33*, 63–67. [\[CrossRef\]](#)
21. Ren, D.C.; Zhang, H.B.; Liu, Y.J.; Li, S.J.; Jin, W.; Yang, R.; Zhang, L.C. Microstructure and properties of equiatomic Ti-Ni alloy fabricated by selective laser melting. *Mater. Sci. Eng. A* **2020**, *771*, 138586. [\[CrossRef\]](#)
22. Zhang, L.-C.; Chen, L.-Y.; Wang, L. Surface modification of titanium and titanium alloys: Technologies, developments and future interests. *Adv. Eng. Mater.* **2020**, *22*, 1901258. [\[CrossRef\]](#)

23. Calin, M.; Zhang, L.C.; Eckert, J. Tailoring of microstructure and mechanical properties of a Ti-based bulk metallic glass-forming alloy. *Scr. Mater.* **2007**, *57*, 1101–1104. [\[CrossRef\]](#)
24. Carman, A.; Zhang, L.C.; Ivasishin, O.M.; Savvakina, D.G.; Matviychuk, M.V.; Pereloma, E.V. Role of alloying elements in microstructure evolution and alloying elements behaviour during sintering of a near- $\beta$  titanium alloy. *Mater. Sci. Eng. A* **2011**, *528*, 1686–1693. [\[CrossRef\]](#)
25. Zhang, L.C.; Klemm, D.; Eckert, J.; Hao, Y.L.; Sercombe, T.B. Manufacture by selective laser melting and mechanical behavior of a biomedical Ti-24Nb-4Zr-8Sn alloy. *Scr. Mater.* **2011**, *65*, 21–24. [\[CrossRef\]](#)
26. Davidson, J.A.; Kovacs, P. Biocompatible Low Modulus Titanium Alloy for Medical Implants. U.S. Patent 5169597, 8 December 1992. No.4.
27. Bottino, M.C.; Coelho, P.G.; Yoshimoto, M.; König, B.; Henriques, V.A.R.; Bressiani, A.H.A.; Bressiani, J.C. Histomorphologic evaluation of Ti-13Nb-13Zr alloys processed via powder metallurgy. *A study in rabbits. Mater. Sci. Eng. C* **2008**, *28*, 223–227. [\[CrossRef\]](#)
28. Bottino, M.C.; Coelho, P.G.; Henriques, V.A.R.; Higa, O.Z.; Bressiani, A.H.A.; Bressiani, J.C. Processing, characterization, and in vitro/in vivo evaluations of powder metallurgy processed Ti-13Nb-13Zr alloys. *J. Biomed. Mater. Res. A* **2009**, *88*, 689–696. [\[CrossRef\]](#)
29. Müller, F.A.; Bottino, M.C.; Müller, L.; Henriques, V.A.R.; Lohbauer, U.; Bressiani, A.H.A.; Bressiani, J.C. In vitro apatite formation on chemically treated (P/M) Ti-13Nb-13Zr. *Dent. Mater.* **2008**, *24*, 50–56. [\[CrossRef\]](#)
30. Henriques, V.A.R.; Galvani, E.T.; Petroni, S.L.G.; Paula, M.S.M.; Lemos, T.G. Production of Ti-13Nb-13Zr alloy for surgical implants by powder metallurgy. *J. Mater. Sci.* **2010**, *45*, 5844–5850. [\[CrossRef\]](#)
31. Niemeyer, T.C.; Grandini, C.R.; Pinto, L.M.C.; Angelo, A.C.D.; Schneider, S.G. Corrosion behavior of Ti-13Nb-13Zr alloy used as a biomaterial. *J. Alloys Compd.* **2009**, *476*, 172–175. [\[CrossRef\]](#)
32. Saji, V.S.; Choe, H.C. Electrochemical corrosion behaviour of nanotubular Ti-13Nb-13Zr alloy in Ringer's solution. *Corros. Sci.* **2009**, *51*, 1658–1663. [\[CrossRef\]](#)
33. Babilas, D.; Urbańczyk, E.; Sowa, M.; Maciej, A.; Korotin, D.M.; Zhidkov, I.S.; Basiaga, M.; Krok-Borkowicz, M.; Szyk-Warszyńska, L.; Pamuła, E. On the electropolishing and anodic oxidation of Ti-15Mo alloy. *Electrochim. Acta* **2016**, *205*, 256–265. [\[CrossRef\]](#)
34. Nag, S.; Banerjee, R.; Fraser, H.L. Microstructural evolution and strengthening mechanisms in Ti-Nb-Zr-Ta, Ti-Mo-Zr-Fe and Ti-15Mo biocompatible alloys. *Mater. Sci. Eng. C* **2005**, *25*, 357–362. [\[CrossRef\]](#)
35. Banerjee, S.; Naik, U.M. Plastic instability in an omega forming Ti-15% Mo alloy. *Acta Mater.* **1996**, *44*, 3667–3677. [\[CrossRef\]](#)
36. Nag, S.; Banerjee, R.; Stechschulte, J.; Fraser, H.L. Comparison of microstructural evolution in Ti-Mo-Zr-Fe and Ti-15Mo biocompatible alloys. *J. Mater. Sci. Mater. Med.* **2005**, *16*, 679–685. [\[CrossRef\]](#)
37. Inaekyan, K.; Brailovski, V.; Prokoshkin, S.; Pushin, V.; Dubinskiy, S.; Sheremetyev, V. Comparative study of structure formation and mechanical behavior of age-hardened Ti-Nb-Zr and Ti-Nb-Ta shape memory alloys. *Mater. Charact.* **2015**, *103*, 65–74. [\[CrossRef\]](#)
38. Tang, X.; Ahmed, T.; Rack, H.J. Phase transformations in Ti-Nb-Ta and Ti-Nb-Ta-Zr alloys. *J. Mater. Sci.* **2000**, *35*, 1805–1811. [\[CrossRef\]](#)
39. Hussein, A.H.; Gepreel, M.A.H.; Gouda, M.K.; Hefnawy, A.M.; Kandil, S.H. Biocompatibility of new Ti-Nb-Ta base alloys. *Mater. Sci. Eng. C* **2016**, *61*, 574–578. [\[CrossRef\]](#)
40. Liu, Y.J.; Li, X.P.; Zhang, L.C.; Sercombe, T.B. Processing and properties of topologically optimised biomedical Ti-24Nb-4Zr-8Sn scaffolds manufactured by selective laser melting. *Mater. Sci. Eng. A* **2015**, *642*, 268–278. [\[CrossRef\]](#)
41. Zhang, L.C.; Sercombe, T.B. Selective Laser Melting of Low-Modulus Biomedical Ti-24Nb-4Zr-8Sn Alloy: Effect of Laser Point Distance. *Key Eng. Mater.* **2012**, *520*, 226–233. [\[CrossRef\]](#)
42. Liu, Y.; Li, S.; Hou, W.; Wang, S.; Hao, Y.; Yang, R.; Sercombe, T.B.; Zhang, L.-C. Electron beam melted beta-type Ti-24Nb-4Zr-8Sn porous structures with high strength-to-modulus ratio. *J. Mater. Sci. Technol.* **2016**, *32*, 505–508. [\[CrossRef\]](#)
43. Bai, Y.; Li, S.J.; Prima, F.; Hao, Y.L.; Yang, R. Electrochemical corrosion behavior of Ti-24Nb-4Zr-8Sn alloy in a simulated physiological environment. *Appl. Surf. Sci.* **2012**, *258*, 4035–4040. [\[CrossRef\]](#)
44. Obbard, E.G.; Hao, Y.L.; Talling, R.J.; Li, S.J.; Zhang, Y.W.; Dye, D.; Yang, R. The effect of oxygen on  $\alpha''$  martensite and superelasticity in Ti-24Nb-4Zr-8Sn. *Acta Mater.* **2011**, *59*, 112–125. [\[CrossRef\]](#)
45. Hafeez, N.; Liu, S.; Lu, E.; Wang, L.; Liu, R.; Lu, W.; Zhang, L.C. Mechanical behavior and phase transformation of  $\beta$ -type Ti-35Nb-2Ta-3Zr alloy fabricated by 3D-Printing. *J. Alloys Compd.* **2019**, *790*, 117–126. [\[CrossRef\]](#)

46. Wang, L.; Xie, L.; Lv, Y.; Zhang, L.-C.; Chen, L.; Meng, Q.; Qu, J.; Zhang, D.; Lu, W. Microstructure evolution and superelastic behavior in Ti-35Nb-2Ta-3Zr alloy processed by friction stir processing. *Acta Mater.* **2017**, *131*, 499–510. [[CrossRef](#)]
47. Wang, L.; Qu, J.; Chen, L.; Meng, Q.; Zhang, L.C.; Qin, J.; Zhang, D.; Lu, W. Investigation of Deformation Mechanisms in  $\beta$ -Type Ti-35Nb-2Ta-3Zr Alloy via FSP Leading to Surface Strengthening. *Metall. Mater. Trans. A* **2015**, *46*, 4813–4818. [[CrossRef](#)]
48. Gu, H.; Ding, Z.; Yang, Z.; Yu, W.; Zhang, W.; Lu, W.; Zhang, L.C.; Wang, K.; Wang, L.; Fu, Y.F. Microstructure evolution and electrochemical properties of TiO<sub>2</sub>/Ti-35Nb-2Ta-3Zr micro/nano-composites fabricated by friction stir processing. *Mater. Des.* **2019**, *169*, 107680. [[CrossRef](#)]
49. Banerjee, R.; Nag, S.; Stechschulte, J.; Fraser, H.L. Strengthening mechanisms in Ti-Nb-Zr-Ta and Ti-Mo-Zr-Fe orthopaedic alloys. *Biomaterials* **2004**, *25*, 3413–3419. [[CrossRef](#)]
50. Zhang, T.; Fan, Q.; Ma, X.; Wang, W.; Wang, K.; Shen, P.; Yang, J. Microstructure and mechanical properties of Ti-35Nb-2Ta-3Zr alloy by laser quenching. *Front. Mater.* **2019**, *6*, 318. [[CrossRef](#)]
51. Saji, V.S.; Choe, H.C.; Brantley, W.A. An electrochemical study on self-ordered nanoporous and nanotubular oxide on Ti-35Nb-5Ta-7Zr alloy for biomedical applications. *Acta Biomater.* **2009**, *5*, 2303–2310. [[CrossRef](#)]
52. Afonso, C.R.M.; Ferrandini, P.L.; Ramirez, A.J.; Caram, R. High resolution transmission electron microscopy study of the hardening mechanism through phase separation in a  $\beta$ -Ti-35Nb-7Zr-5Ta alloy for implant applications. *Acta Biomater.* **2010**, *6*, 1625–1629. [[CrossRef](#)] [[PubMed](#)]
53. Zou, L.M.; Yang, C.; Long, Y.; Xiao, Z.Y.; Li, Y.Y. Fabrication of biomedical Ti-35Nb-7Zr-5Ta alloys by mechanical alloying and spark plasma sintering. *Powder Metall.* **2012**, *55*, 65–70. [[CrossRef](#)]
54. Yang, K.; Wang, J.; Tang, H.; Li, Y. Additive manufacturing of in-situ reinforced Ti-35Nb-5Ta-7Zr (TNTZ) alloy by selective electron beam melting (SEBM). *J. Alloys Compd.* **2020**, *826*, 154178. [[CrossRef](#)]
55. Salvador, C.A.F.; Lopes, E.S.N.; Ospina, C.A.; Caram, R. Orthorhombic martensite formation upon aging in a Ti-30Nb-4Sn alloy. *Mater. Chem. Phys.* **2016**, *183*, 238–246. [[CrossRef](#)]
56. Fanton, L.; de Lima, N.B.; de Oliveira França Hayama, A.; Caram, R.; Fogagnolo, J.B. Texture Development in Cold Deformed and Recrystallized Ti-30Nb-4Sn Alloy and its effects on hardness and Young's modulus. *Adv. Eng. Mater.* **2017**, *19*, 1600058. [[CrossRef](#)]
57. Wang, J.C.; Liu, Y.J.; Qin, P.; Liang, S.X.; Sercombe, T.B.; Zhang, L.C. Selective laser melting of Ti-35Nb composite from elemental powder mixture: Microstructure, mechanical behavior and corrosion behavior. *Mater. Sci. Eng. A* **2019**, *760*, 214–224. [[CrossRef](#)]
58. Karre, R.; Niranjana, M.K.; Dey, S.R. First principles theoretical investigations of low Young's modulus beta Ti-Nb and Ti-Nb-Zr alloys compositions for biomedical applications. *Mater. Sci. Eng. C* **2015**, *50*, 52–58. [[CrossRef](#)]
59. Verissimo, N.C.; Figueiredo, R.S.; de Oliveira, H.G.; Rodrigues, C.A.; Caram, R.; Bertazzoli, R. Characterization of the photoactivity of nanotube layers grown on Ti-35Nb and Ti-35Nb-4Sn alloys. *J. Mater. Sci.* **2016**, *51*, 9384–9393. [[CrossRef](#)]
60. Santos, D.R.; Pereira, M.D.S.; Cairo, C.A.A.; Graca, M.L.A.; Henriques, V.A.R. Isochronal sintering of the blended elemental Ti-35Nb alloy. *Mater. Sci. Eng. A* **2008**, *472*, 193–197. [[CrossRef](#)]
61. Liu, Y.J.; Zhang, Y.S.; Zhang, L.C. Transformation-induced plasticity and high strength in beta titanium alloy manufactured by selective laser melting. *Materialia* **2019**, *6*, 100299. [[CrossRef](#)]
62. Bai, X.F.; Zhao, Y.Q.; Jia, Z.Q.; Zhang, Y.S.; Li, B. Grain boundary character distribution of TLM titanium alloy during deformation. *J. Mater. Eng. Perform.* **2016**, *25*, 2236–2244. [[CrossRef](#)]
63. Yu, Z.-T.; Zheng, Y.-F.; Niu, J.-L.; Huangfu, Q.; Zhang, Y.-F.; Yu, S. Microstructure and wear resistance of Ti-3Zr-2Sn-3Mo-15Nb (TLM) alloy. *Trans. Nonfer. Metall. Soc. China* **2007**, *17*, s495–s499.
64. Zhentao, Y.; Lian, Z. Influence of martensitic transformation on mechanical compatibility of biomedical  $\beta$  type titanium alloy TLM. *Mater. Sci. Eng. A* **2006**, *438*, 391–394. [[CrossRef](#)]
65. Choubey, A.; Balasubramaniam, R.; Basu, B. Effect of replacement of V by Nb and Fe on the electrochemical and corrosion behavior of Ti-6Al-4V in simulated physiological environment. *J. Alloys Compd.* **2004**, *381*, 288–294. [[CrossRef](#)]
66. Oliveira, N.T.C.; Aleixo, G.; Caram, R.; Guastaldi, A.C. Development of Ti-Mo alloys for biomedical applications: Microstructure and electrochemical characterization. *Mater. Sci. Eng. A* **2007**, *452*, 727–731. [[CrossRef](#)]

67. Yang, X.; Hutchinson, C.R. Corrosion-wear of beta-Ti alloy TMZF (Ti-12Mo-6Zr-2Fe) in simulated body fluid. *Acta Biomater.* **2016**, *42*, 429–439. [[CrossRef](#)]
68. Ishimoto, T.; Hagihara, K.; Hisamoto, K.; Sun, S.-H.; Nakano, T. Crystallographic texture control of beta-type Ti-15Mo-5Zr-3Al alloy by selective laser melting for the development of novel implants with a biocompatible low Young's modulus. *Scr. Mater.* **2017**, *132*, 34–38. [[CrossRef](#)]
69. Lakshmi, R.V.; Bera, P.; Anandan, C. Surface treatment and its effect on the electrochemical behavior of Ti-15Mo-3Nb-3Al alloy. *RSC Adv.* **2016**, *6*, 36345–36355. [[CrossRef](#)]
70. Gordin, D.M.; Gloriant, T.; Texier, G.; Thibon, I.; Ansel, D.; Duval, J.L.; Nagel, M.D. Development of a  $\beta$ -type Ti-12Mo-5Ta alloy for biomedical applications: Cytocompatibility and metallurgical aspects. *J. Mater. Sci. Mater. Med.* **2004**, *15*, 885–891. [[CrossRef](#)] [[PubMed](#)]
71. Zhang, L.C.; Das, J.; Lu, H.B.; Duhamel, C.; Calin, M.; Eckert, J. High strength Ti-Fe-Sn ultrafine composites with large plasticity. *Scr. Mater.* **2007**, *57*, 101–104. [[CrossRef](#)]
72. Haghighi, S.E.; Lu, H.B.; Jian, G.Y.; Cao, G.H.; Habibi, D.; Zhang, L.C. Effect of  $\alpha''$  martensite on the microstructure and mechanical properties of beta-type Ti-Fe-Ta alloys. *Mater. Des.* **2015**, *76*, 47–54. [[CrossRef](#)]
73. Ehtemam-Haghighi, S.; Cao, G.; Zhang, L.-C. Nanoindentation study of mechanical properties of Ti based alloys with Fe and Ta additions. *J. Alloys Compd.* **2017**, *692*, 892–897. [[CrossRef](#)]
74. Ehtemam-Haghighi, S.; Liu, Y.; Cao, G.; Zhang, L.-C. Influence of Nb on the  $\beta \rightarrow \alpha''$  martensitic phase transformation and properties of the newly designed Ti-Fe-Nb alloys. *Mater. Sci. Eng. C* **2016**, *60*, 503–510. [[CrossRef](#)] [[PubMed](#)]
75. Ehtemam-Haghighi, S.; Prashanth, K.G.; Attar, H.; Chaubey, A.K.; Cao, G.H.; Zhang, L.C. Evaluation of mechanical and wear properties of Ti-xNb-7Fe alloys designed for biomedical applications. *Mater. Des.* **2016**, *111*, 592–599. [[CrossRef](#)]
76. Ehtemam-Haghighi, S.; Liu, Y.; Cao, G.; Zhang, L.C. Phase transition, microstructural evolution and mechanical properties of Ti-Nb-Fe alloys induced by Fe addition. *Mater. Des.* **2016**, *97*, 279–286. [[CrossRef](#)]
77. Rabadia, C.D.; Liu, Y.J.; Wang, L.; Sun, H.; Zhang, L.C. Laves phase precipitation in Ti-Zr-Fe-Cr alloys with high strength and large plasticity. *Mater. Des.* **2018**, *154*, 228–238. [[CrossRef](#)]
78. Rabadia, C.D.; Liu, Y.J.; Chen, L.Y.; Jawed, S.F.; Wang, L.Q.; Sun, H.; Zhang, L.C. Deformation and strength characteristics of Laves phases in titanium alloys. *Mater. Des.* **2019**, *179*, 107891. [[CrossRef](#)]
79. Jawed, S.F.; Rabadia, C.D.; Liu, Y.J.; Wang, L.Q.; Li, Y.H.; Zhang, X.H.; Zhang, L.C. Beta-type Ti-Nb-Zr-Cr alloys with large plasticity and significant strain hardening. *Mater. Des.* **2019**, *181*, 108064. [[CrossRef](#)]
80. Kumar, S.; Sankara Narayanan, T.S.N. Electrochemical characterization of  $\beta$ -Ti alloy in Ringer's solution for implant application. *J. Alloys Compd.* **2009**, *479*, 699–703. [[CrossRef](#)]
81. Afonso, C.R.M.; Chaves, J.M.; Florêncio, O. Effect of rapid solidification on microstructure and elastic modulus of  $\beta$  Ti-xNb-3Fe alloys for implant applications. *Adv. Eng. Mater.* **2017**, *19*, 1600370.
82. Amigó, A.; Vicente, A.; Afonso, C.; Amigó, V. Mechanical properties and the microstructure of  $\beta$  Ti-35Nb-10Ta-xFe alloys obtained by powder metallurgy for biomedical applications. *Metals* **2019**, *9*, 76. [[CrossRef](#)]
83. Chen, L.; Li, J.; Zhang, Y.; Zhang, L.C.; Lu, W.; Wang, L.; Zhang, L.; Zhang, D. Zr-Sn-Nb-Fe-Si-O alloy for fuel cladding candidate: Processing, microstructure, corrosion resistance and tensile behavior. *Corros. Sci.* **2015**, *100*, 332–340. [[CrossRef](#)]
84. Chen, L.Y.; Shen, P.; Zhang, L.; Lu, S.; Chai, L.; Yang, Z.; Zhang, L.C. Corrosion behavior of non-equilibrium Zr-Sn-Nb-Fe-Cu-O alloys in high-temperature 0.01 M LiOH aqueous solution and degradation of the surface oxide films. *Corros. Sci.* **2018**, *136*, 221–230. [[CrossRef](#)]
85. Chai, L.J.; Wang, S.Y.; Wu, H.; Guo, N.; Pan, H.C.; Chen, L.Y.; Murty, K.L.; Song, B.  $\alpha \rightarrow \beta$  Transformation characteristics revealed by pulsed laser-induced non-equilibrium microstructures in duplex-phase Zr alloy. *Sci. China Technol. Sci.* **2017**, *60*, 1255–1262. [[CrossRef](#)]
86. Zhang, M.; Li, Y.N.; Zhang, F.C.; Wang, X.B.; Chen, L.Y.; Yang, Z.N. Effect of annealing treatment on the microstructure and mechanical properties of a duplex Zr-2.5 Nb alloy. *Mater. Sci. Eng. A* **2017**, *706*, 236–241. [[CrossRef](#)]
87. Fisher, E.S.; Renken, C.J. Single-crystal elastic moduli and the hcp  $\rightarrow$  bcc transformation in Ti, Zr, and Hf. *Phys. Rev.* **1964**, *135*, A482. [[CrossRef](#)]
88. Kuroda, D.; Niinomi, M.; Morinaga, M.; Kato, Y.; Yashiro, T. Design and mechanical properties of new  $\beta$  type titanium alloys for implant materials. *Mater. Sci. Eng. A* **1998**, *243*, 244–249. [[CrossRef](#)]



89. Niinomi, M.; Kuroda, D.; Fukunaga, K.-i.; Morinaga, M.; Kato, Y.; Yashiro, T.; Suzuki, A. Corrosion wear fracture of new  $\beta$  type biomedical titanium alloys. *Mater. Sci. Eng. A* **1999**, *263*, 193–199. [[CrossRef](#)]
90. Moffat, D.L.; Kattner, U.R. The stable and metastable Ti-Nb phase diagrams. *Metall. Trans. A* **1988**, *19*, 2389–2397. [[CrossRef](#)]
91. Murray, J.L. The Mo–Ti (molybdenum-titanium) system. *Bull. Alloys Phase Diagr.* **1981**, *2*, 185–192. [[CrossRef](#)]
92. Min, X.; Chen, X.; Emura, S.; Tsuchiya, K. Mechanism of twinning-induced plasticity in  $\beta$ -type Ti–15Mo alloy. *Scr. Mater.* **2013**, *69*, 393–396. [[CrossRef](#)]
93. Ho, W.F.; Ju, C.-P.; Lin, J.H.C. Structure and properties of cast binary Ti–Mo alloys. *Biomaterials* **1999**, *20*, 2115–2122. [[CrossRef](#)]
94. Cvijović-Alagić, I.; Cvijović, Z.; Mitrović, S.; Panić, V.; Rakin, M. Wear and corrosion behaviour of Ti–13Nb–13Zr and Ti–6Al–4V alloys in simulated physiological solution. *Corros. Sci.* **2011**, *53*, 796–808. [[CrossRef](#)]
95. Milošev, I.; Žerjav, G.; Moreno, J.M.C.; Popa, M. Electrochemical properties, chemical composition and thickness of passive film formed on novel Ti–20Nb–10Zr–5Ta alloy. *Electrochim. Acta* **2013**, *99*, 176–189. [[CrossRef](#)]
96. Goldberg, A.J.; Shastri, C.V. Age hardening of orthodontic beta titanium alloys. *J. Biomed. Mater. Res.* **1984**, *18*, 155–163. [[CrossRef](#)]
97. Hanada, S.; Izumi, O. Correlation of tensile properties, deformation modes, and phase stability in commercial  $\beta$ -phase titanium alloys. *Metall. Mater. Trans. A* **1987**, *18*, 265–271. [[CrossRef](#)]
98. Qazi, J.I.; Marquardt, B.; Allard, L.F.; Rack, H.J. Phase transformations in Ti–35Nb–7Zr–5Ta–(0.06–0.68) O alloys. *Mater. Sci. Eng. C* **2005**, *25*, 389–397. [[CrossRef](#)]
99. Niinomi, M. Fatigue performance and cyto-toxicity of low rigidity titanium alloy, Ti–29Nb–13Ta–4.6Zr. *Biomaterials* **2003**, *24*, 2673–2683. [[CrossRef](#)]
100. Santos, P.F.; Niinomi, M.; Liu, H.; Cho, K.; Nakai, M.; Trenggono, A.; Champagne, S.; Hermawan, H.; Narushima, T. Improvement of microstructure, mechanical and corrosion properties of biomedical Ti–Mn alloys by Mo addition. *Mater. Des.* **2016**, *110*, 414–424. [[CrossRef](#)]
101. Niinomi, M. Mechanical properties of biomedical titanium alloys. *Mater. Sci. Eng. A* **1998**, *243*, 231–236. [[CrossRef](#)]
102. Popa, M.; Vasilescu, E.; Drob, P.; Raducanu, D.; Moreno, J.M.C.; Ivanescu, S.; Vasilescu, C.; Drob, S.I. Microstructure, mechanical, and anticorrosive properties of a new Ti–20Nb–10Zr–5Ta alloy based on nontoxic and nonallergenic elements. *Met. Mater. Int.* **2012**, *18*, 639–645. [[CrossRef](#)]
103. Matsumoto, H.; Watanabe, S.; Hanada, S.  $\alpha'$  Martensite Ti–V–Sn alloys with low Young’s modulus and high strength. *Mater. Sci. Eng. A* **2007**, *448*, 39–48. [[CrossRef](#)]
104. Jawed, S.F.; Rabadia, C.D.; Liu, Y.J.; Wang, L.Q.; Qin, P.; Li, Y.H.; Zhang, X.H.; Zhang, L.C. Strengthening mechanism and corrosion resistance of beta-type Ti–Nb–Zr–Mn alloys. *Mater. Sci. Eng. C* **2020**, *110*, 110728. [[CrossRef](#)] [[PubMed](#)]
105. Jawed, S.F.; Rabadia, C.D.; Liu, Y.J.; Wang, L.Q.; Li, Y.H.; Zhang, X.H.; Zhang, L.C. Mechanical characterization and deformation behavior of  $\beta$ -stabilized Ti–Nb–Sn–Cr alloys. *J. Alloys Compd.* **2019**, *792*, 684–693. [[CrossRef](#)]
106. Tamirisakandala, S.; Bhat, R.B.; Tiley, J.S.; Miracle, D.B. Processing, microstructure, and properties of  $\beta$  titanium alloys modified with boron. *J. Mater. Eng. Perform.* **2005**, *14*, 741–746. [[CrossRef](#)]
107. Yadav, P.; Saxena, K.K. Effect of heat-treatment on microstructure and mechanical properties of Ti alloys: An overview. *Mater. Today Proc.* **2020**, *26*, 2546–2557. [[CrossRef](#)]
108. Rabadia, C.D.; Liu, Y.J.; Cao, G.H.; Li, Y.H.; Zhang, C.W.; Sercombe, T.B.; Sun, H.; Zhang, L.C. High-strength  $\beta$  stabilized Ti–Nb–Fe–Cr alloys with large plasticity. *Mater. Sci. Eng. A* **2018**, *732*, 368–377. [[CrossRef](#)]
109. Morinaga, M.; Yukawa, N.; Maya, T.; Sone, K.; Adachi, H. Theoretical design of titanium alloys. In Proceedings of the 6th World Conference on Titanium III, Cannes, France, 6–9 June 1988; Societe Francaise de Metallurgie: Paris, France, 1988; pp. 1601–1606.
110. Okamoto, H. *Phase Diagrams for Binary Alloys*, 2nd ed.; ASM international: Metals Park, OH, USA, 2010; Volume 314.
111. Morinaga, M.; Kato, M.; Kimura, T.; Fukumoto, M.; Harada, I.; Kubo, K. Theoretical design of  $\beta$ -type titanium alloys. In Proceedings of the 7th World Conference on Titanium, Warrendale, PA, USA, 29 June–2 July 1992; pp. 217–224.



112. Marteleur, M.; Sun, F.; Gloriant, T.; Vermaut, P.; Jacques, P.J.; Prima, F. On the design of new  $\beta$ -metastable titanium alloys with improved work hardening rate thanks to simultaneous TRIP and TWIP effects. *Scr. Mater.* **2012**, *66*, 749–752. [\[CrossRef\]](#)
113. Weiss, I.; Semiatin, S.L. Thermomechanical processing of beta titanium alloys—An overview. *Mater. Sci. Eng. A* **1998**, *243*, 46–65. [\[CrossRef\]](#)
114. Chirico, C.; Tsipas, S.A.; Wilczynski, P.; Gordo, E. Beta Titanium Alloys Produced from Titanium Hydride: Effect of Alloying Elements on Titanium Hydride Decomposition. *Metals* **2020**, *10*, 682. [\[CrossRef\]](#)
115. Liu, Y.J.; Li, S.J.; Wang, H.L.; Hou, W.T.; Hao, Y.L.; Yang, R.; Sercombe, T.B.; Zhang, L.C. Microstructure, defects and mechanical behavior of beta-type titanium porous structures manufactured by electron beam melting and selective laser melting. *Acta Mater.* **2016**, *113*, 56–67. [\[CrossRef\]](#)
116. Liu, Y.J.; Ren, D.C.; Li, S.J.; Wang, H.; Zhang, L.C.; Sercombe, T.B. Enhanced fatigue characteristics of a topology-optimized porous titanium structure produced by selective laser melting. *Addit. Manuf.* **2020**, *32*, 101060. [\[CrossRef\]](#)
117. Zhang, L.-C.; Xu, J.; Eckert, J. Thermal stability and crystallization kinetics of mechanically alloyed TiC/Ti-based metallic glass matrix composite. *J. Appl. Phys.* **2006**, *100*, 033514. [\[CrossRef\]](#)
118. Oh, I.-H.; Nomura, N.; Masahashi, N.; Hanada, S. Mechanical properties of porous titanium compacts prepared by powder sintering. *Scr. Mater.* **2003**, *49*, 1197–1202. [\[CrossRef\]](#)
119. Krishna, B.V.; Bose, S.; Bandyopadhyay, A. Low stiffness porous Ti structures for load-bearing implants. *Acta Biomater.* **2007**, *3*, 997–1006. [\[CrossRef\]](#)
120. Au, A.G.; Raso, V.J.; Liggins, A.B.; Amirfazli, A. Contribution of loading conditions and material properties to stress shielding near the tibial component of total knee replacements. *J. Biomech.* **2007**, *40*, 1410–1416. [\[CrossRef\]](#)
121. Huiskes, R.; Weinans, H.; Van Rietbergen, B. The relationship between stress shielding and bone resorption around total hip stems and the effects of flexible materials. *Clin. Orthop. Relat. Res.* **1992**, *274*, 124–134. [\[CrossRef\]](#)
122. Nagels, J.; Stokdijk, M.; Rozing, P.M. Stress shielding and bone resorption in shoulder arthroplasty. *J. Shoulder Elb. Surg.* **2003**, *12*, 35–39. [\[CrossRef\]](#)
123. Pałka, K.; Pokrowiecki, R. Porous titanium implants: A review. *Adv. Eng. Mater.* **2018**, *20*, 1700648. [\[CrossRef\]](#)
124. Yang, C.; Kang, L.M.; Li, X.X.; Zhang, W.W.; Zhang, D.T.; Fu, Z.Q.; Li, Y.Y.; Zhang, L.C.; Lavernia, E.J. Bimodal titanium alloys with ultrafine lamellar eutectic structure fabricated by semi-solid sintering. *Acta Mater.* **2017**, *132*, 491–502. [\[CrossRef\]](#)
125. Sudha, G.T.; Stalin, B.; Ravichandran, M.; Balasubramanian, M. Mechanical Properties, characterization and wear behavior of powder metallurgy composites—A review. *Mater. Today Proc.* **2020**, *22*, 2582–2596. [\[CrossRef\]](#)
126. Tong, H.; Qiu, F.; Zuo, R.; Shen, P.; Cong, X.; Liu, J.; Yang, H.; Jiang, Q. The effect and mechanism of alloying elements on Al/SiC interfacial reaction in Al melt. *Appl. Surf. Sci.* **2020**, *501*, 144265. [\[CrossRef\]](#)
127. Guo, P.Y.; Sun, H.; Shao, Y.; Ding, J.T.; Li, J.C.; Huang, M.R.; Mao, S.Y.; Wang, Y.X.; Zhang, J.F.; Long, R.C. The evolution of microstructure and electrical performance in doped Mn-Co and Cu-Mn oxide layers with the extended oxidation time. *Corros. Sci.* **2020**, 108738. [\[CrossRef\]](#)
128. Dong, B.-X.; Yang, H.-Y.; Qiu, F.; Li, Q.; Shu, S.-L.; Zhang, B.-Q.; Jiang, Q.-C. Design of TiC nanoparticles and their morphology manipulating mechanisms by stoichiometric ratios: Experiment and first-principle calculation. *Mater. Des.* **2019**, *181*, 107951. [\[CrossRef\]](#)
129. Yang, H.-Y.; Wang, Z.; Yue, X.; Ji, P.-J.; Shu, S.-L. Simultaneously improved strength and toughness of in situ bi-phased TiB<sub>2</sub>-Ti(C,N)-Ni cermets by Mo addition. *J. Alloys Compd.* **2019**, *820*, 153068. [\[CrossRef\]](#)
130. Li, Q.; Qiu, F.; Dong, B.-X.; Gao, X.; Shu, S.-L.; Yang, H.-Y.; Jiang, Q.-C. Processing, multiscale microstructure refinement and mechanical property enhancement of hypoeutectic Al-Si alloys via in situ bimodal-sized TiB<sub>2</sub> particles. *Mater. Sci. Eng. A* **2020**, *777*, 139081. [\[CrossRef\]](#)
131. Dercz, G.; Matuła, I.; Zubko, M.; Kazek-Kęsik, A.; Maszybrocka, J.; Simka, W.; Dercz, J.; Świec, P.; Jendrzejewska, I. Synthesis of porous Ti-50Ta alloy by powder metallurgy. *Mater. Charact.* **2018**, *142*, 124–136. [\[CrossRef\]](#)
132. Yang, H.-Y.; Wang, Z.; Shu, S.-L.; Lu, J.-B. Effect of Ta addition on the microstructures and mechanical properties of in situ bi-phase (TiB<sub>2</sub>-TiC<sub>x</sub>Ny)/(Ni-Ta) cermets. *Ceram. Int.* **2020**, *45*, 4408–4417. [\[CrossRef\]](#)

133. Lin, Q.; Yang, F.; Yang, H.; Sui, R.; Shi, Y.; Wang, J. Wetting of graphite by molten Cu-xSn-yCr ternary alloys at 1373 K. *Carbon* **2020**, *159*, 561–569. [[CrossRef](#)]
134. Zhang, L.C.; Xu, J. Glass-forming ability of melt-spun multicomponent (Ti, Zr, Hf)–(Cu, Ni, Co)–Al alloys with equiatomic substitution. *J. Non-Cryst. Solids* **2004**, *347*, 166–172. [[CrossRef](#)]
135. Zhang, L.C.; Xu, J.; Ma, E. Consolidation and properties of ball-milled Ti50Cu18Ni22Al4Sn6 glassy alloy by equal channel angular extrusion. *Mater. Sci. Eng. A* **2006**, *434*, 280–288. [[CrossRef](#)]
136. Liu, L.H.; Yang, C.; Kang, L.M.; Long, Y.; Xiao, Z.Y.; Li, P.J.; Zhang, L.C. Equiaxed Ti-based composites with high strength and large plasticity prepared by sintering and crystallizing amorphous powder. *Mater. Sci. Eng. A* **2016**, *650*, 171–182. [[CrossRef](#)]
137. Torres, Y.; Pavón, J.J.; Nieto, I.; Rodríguez, J.A. Conventional powder metallurgy process and characterization of porous titanium for biomedical applications. *Metall. Mater. Trans. B* **2011**, *42*, 891–900. [[CrossRef](#)]
138. Wang, H.; Fang, Z.Z.; Sun, P. A critical review of mechanical properties of powder metallurgy titanium. *Int. J. Powder Metall.* **2010**, *46*, 45–57.
139. Yamanoglu, R.; Gulsoy, N.; Olevsky, E.A.; Gulsoy, H.O. Production of porous Ti5Al2.5Fe alloy via pressureless spark plasma sintering. *J. Alloys Compd.* **2016**, *680*, 654–658. [[CrossRef](#)]
140. Hussein, M.A.; Suryanarayana, C.; Al-Aqeeli, N. Fabrication of nano-grained Ti–Nb–Zr biomaterials using spark plasma sintering. *Mater. Des.* **2015**, *87*, 693–700. [[CrossRef](#)]
141. Muñoz, S.; Pavón, J.; Rodríguez-Ortiz, J.A.; Civantos, A.; Allain, J.P.; Torres, Y. On the influence of space holder in the development of porous titanium implants: Mechanical, computational and biological evaluation. *Mater. Charact.* **2015**, *105*, 68–78. [[CrossRef](#)]
142. Arifvianto, B.; Zhou, J. Fabrication of metallic biomedical scaffolds with the space holder method: A review. *Materials* **2014**, *7*, 3588–3622. [[CrossRef](#)]
143. Zhang, L.C.; Shen, Z.Q.; Xu, J. Mechanically milling-induced amorphization in Sn-containing Ti-based multicomponent alloy systems. *Mater. Sci. Eng. A* **2005**, *394*, 204–209. [[CrossRef](#)]
144. Zhang, L.C.; Xu, J.; Ma, E. Mechanically alloyed amorphous Ti50(Cu0.45Ni0.55)44–xAlxSi4B2 alloys with supercooled liquid region. *J. Mater. Res.* **2002**, *17*, 1743–1749. [[CrossRef](#)]
145. Wang, X.; Li, Y.; Xiong, J.; Hodgson, P.D.; Wen, C.E. Porous TiNbZr alloy scaffolds for biomedical applications. *Acta Biomater.* **2009**, *5*, 3616–3624. [[CrossRef](#)] [[PubMed](#)]
146. Wang, X.H.; Li, S.J.; Jia, M.T.; Hao, Y.L.; Yang, R.; Guo, Z.X. Porous Ti-24Nb-4Zr-8Sn alloy for biomedical applications fabricated by space-holder method. *Chin. J. Nonferr. Met.* **2010**, *20*, s967–s971.
147. Li, B.Q.; Xie, R.Z.; Lu, X. Microstructure, mechanical property and corrosion behavior of porous Ti–Ta–Nb–Zr. *Bioact. Mater.* **2020**, *5*, 564–568. [[CrossRef](#)] [[PubMed](#)]
148. Wong, K.V.; Hernandez, A. A review of additive manufacturing. *Mech. Eng.* **2012**, *2012*, 1–10. [[CrossRef](#)]
149. Liang, S.-X.; Wang, X.; Zhang, W.; Liu, Y.-J.; Wang, W.; Zhang, L.-C. Selective laser melting manufactured porous Fe-based metallic glass matrix composite with remarkable catalytic activity and reusability. *Appl. Mater. Today* **2020**, *19*, 100543. [[CrossRef](#)]
150. Liu, S.; Liu, J.; Wang, L.; Ma, R.L.W.; Zhong, Y.; Lu, W.; Zhang, L.C. Superelastic behavior of in-situ eutectic-reaction manufactured high strength 3D porous NiTi-Nb scaffold. *Scr. Mater.* **2020**, *181*, 121–126. [[CrossRef](#)]
151. Chen, L.-Y.; Xu, T.; Wang, H.; Sang, P.; Lu, S.; Wang, Z.-X.; Chen, S.; Zhang, L.-C. Phase interaction induced texture in a plasma sprayed-remelted NiCrBSi coating during solidification: An electron backscatter diffraction study. *Surf. Coat. Technol.* **2019**, *358*, 467–480. [[CrossRef](#)]
152. Zhang, L.-C.; Liu, Y.; Li, S.; Hao, Y. Additive manufacturing of titanium alloys by electron beam melting: A review. *Adv. Eng. Mater.* **2018**, *20*, 1700842. [[CrossRef](#)]
153. Chai, L.; Chen, K.; Zhi, Y.; Murty, K.L.; Chen, L.Y.; Yang, Z. Nanotwins induced by pulsed laser and their hardening effect in a Zr alloy. *J. Alloys Compd.* **2018**, *748*, 163–170. [[CrossRef](#)]
154. Lu, H.Z.; Yang, C.; Luo, X.; Ma, H.W.; Song, B.; Li, Y.Y.; Zhang, L.C. Ultrahigh-performance TiNi shape memory alloy by 4D printing. *Mater. Sci. Eng. A* **2019**, *763*, 138166. [[CrossRef](#)]
155. Attar, H.; Ehtemam-Haghighi, S.; Soro, N.; Kent, D.; Dargusch, M.S. Additive manufacturing of low-cost porous titanium-based composites for biomedical applications: Advantages, challenges and opinion for future development. *J. Alloys Compd.* **2020**, *827*, 154263. [[CrossRef](#)]
156. Zhang, L.-C.; Attar, H. Selective laser melting of titanium alloys and titanium matrix composites for biomedical applications: A review. *Adv. Eng. Mater.* **2016**, *18*, 463–475. [[CrossRef](#)]

157. Qin, P.; Chen, Y.; Liu, Y.-J.; Zhang, J.; Chen, L.-Y.; Li, Y.; Zhang, X.; Cao, C.; Sun, H.; Zhang, L.-C. Resemblance in corrosion behavior of selective laser melted and traditional monolithic  $\beta$  Ti-24Nb-4Zr-8Sn alloy. *ACS Biomater. Sci. Eng.* **2019**, *5*, 1141–1149. [\[CrossRef\]](#)
158. Bai, Y.; Gai, X.; Li, S.; Zhang, L.-C.; Liu, Y.; Hao, Y.; Zhang, X.; Yang, R.; Gao, Y. Improved corrosion behaviour of electron beam melted Ti-6Al-4V alloy in phosphate buffered saline. *Corros. Sci.* **2017**, *123*, 289–296. [\[CrossRef\]](#)
159. Liu, Y.J.; Li, S.J.; Zhang, L.C.; Hao, Y.L.; Sercombe, T.B. Early plastic deformation behaviour and energy absorption in porous  $\beta$ -type biomedical titanium produced by selective laser melting. *Scr. Mater.* **2018**, *153*, 99–103. [\[CrossRef\]](#)
160. Hafeez, N.; Liu, J.; Wang, L.; Wei, D.; Tang, Y.; Lu, W.; Zhang, L.-C. Superelastic response of low-modulus porous beta-type Ti-35Nb-2Ta-3Zr alloy fabricated by laser powder bed fusion. *Addit. Manuf.* **2020**, *34*, 101264.
161. Wang, J.; Liu, Y.; Rabadia, C.D.; Liang, S.-X.; Sercombe, T.B.; Zhang, L.-C. Microstructural homogeneity and mechanical behavior of a selective laser melted Ti-35Nb alloy produced from an elemental powder mixture. *J. Mater. Sci. Technol.* **2021**, *61*, 221–233. [\[CrossRef\]](#)
162. Speirs, M.; Humbeeck, J.V.; Schrooten, J.; Luyten, J.; Kruth, J.P. The effect of pore geometry on the mechanical properties of selective laser melted Ti-13Nb-13Zr scaffolds. *Procedia Cirp* **2013**, *5*, 79–82. [\[CrossRef\]](#)
163. Thijs, L.; Verhaeghe, F.; Craeghs, T.; Van Humbeeck, J.; Kruth, J.-P. A study of the microstructural evolution during selective laser melting of Ti-6Al-4V. *Acta Mater.* **2010**, *58*, 3303–3312. [\[CrossRef\]](#)
164. Chen, K.; Zeng, L.; Li, Z.; Chai, L.; Wang, Y.; Chen, L.-Y.; Yu, H. Effects of laser surface alloying with Cr on microstructure and hardness of commercial purity Zr. *J. Alloys Compd.* **2019**, *784*, 1106–1112. [\[CrossRef\]](#)
165. Zhao, D.; Han, C.; Li, J.; Liu, J.; Wei, Q. In situ fabrication of a titanium-niobium alloy with tailored microstructures, enhanced mechanical properties and biocompatibility by using selective laser melting. *Mater. Sci. Eng. C* **2020**, *111*, 110784. [\[CrossRef\]](#) [\[PubMed\]](#)
166. Vrancken, B.; Thijs, L.; Kruth, J.P.; Van Humbeeck, J. Microstructure and mechanical properties of a novel  $\beta$  titanium metallic composite by selective laser melting. *Acta Mater.* **2014**, *68*, 150–158. [\[CrossRef\]](#)
167. Fischer, M.; Joguet, D.; Robin, G.; Peltier, L.; Laheurte, P. In situ elaboration of a binary Ti-26Nb alloy by selective laser melting of elemental titanium and niobium mixed powders. *Mater. Sci. Eng. C* **2016**, *62*, 852–859. [\[CrossRef\]](#) [\[PubMed\]](#)
168. Wang, Q.; Han, C.; Choma, T.; Wei, Q.; Yan, C.; Song, B.; Shi, Y. Effect of Nb content on microstructure, property and in vitro apatite-forming capability of Ti-Nb alloys fabricated via selective laser melting. *Mater. Des.* **2017**, *126*, 268–277. [\[CrossRef\]](#)
169. Sing, S.L.; Yeong, W.Y.; Wiria, F.E. Selective laser melting of titanium alloy with 50 wt.% tantalum: Microstructure and mechanical properties. *J. Alloys Compd.* **2016**, *660*, 461–470. [\[CrossRef\]](#)
170. Sing, S.L.; Wiria, F.E.; Yeong, W.Y. Selective laser melting of titanium alloy with 50 wt.% tantalum: Effect of laser process parameters on part quality. *Int. J. Refract. Met. Hard Mater.* **2018**, *77*, 120–127. [\[CrossRef\]](#)
171. Chen, W.; Chen, C.; Zi, X.; Cheng, X.; Zhang, X.; Lin, Y.C.; Zhou, K. Controlling the microstructure and mechanical properties of a metastable  $\beta$  titanium alloy by selective laser melting. *Mater. Sci. Eng. A* **2018**, *726*, 240–250. [\[CrossRef\]](#)
172. Gao, J.J.; Thibon, I.; Castany, P.; Gloriant, T. Effect of grain size on the recovery strain in a new Ti-20Zr-12Nb-2Sn superelastic alloy. *Mater. Sci. Eng. A* **2020**, *793*, 139878. [\[CrossRef\]](#)
173. Schwab, H.; Prashanth, K.G.; Löber, L.; Kühn, U.; Eckert, J. Selective laser melting of Ti-45Nb alloy. *Metals* **2015**, *5*, 686–694. [\[CrossRef\]](#)
174. Li, Y.; Ding, Y.; Munir, K.; Lin, J.; Brandt, M.; Atrens, A.; Xiao, Y.; Kanwar, R.J.; Wen, C. Novel  $\beta$ -Ti35Zr28Nb alloy scaffolds manufactured using selective laser melting for bone implant applications. *Acta Biomater.* **2019**, *87*, 273–284. [\[CrossRef\]](#)
175. Zhou, L.; Yuan, T.; Li, R.; Tang, J.; Wang, M.; Mei, F. Anisotropic mechanical behavior of biomedical Ti-13Nb-13Zr alloy manufactured by selective laser melting. *J. Alloys Compd.* **2018**, *762*, 289–300. [\[CrossRef\]](#)
176. Gokuldoss, P.K.; Kolla, S.; Eckert, J. Additive manufacturing processes: Selective laser melting, electron beam melting and binder jetting—Selection guidelines. *Materials* **2017**, *10*, 672. [\[CrossRef\]](#) [\[PubMed\]](#)
177. Chen, L.-Y.; Wang, H.; Zhao, C.; Lu, S.; Wang, Z.-X.; Sha, J.; Chen, S.; Zhang, L.-C. Automatic remelting and enhanced mechanical performance of a plasma sprayed NiCrBSi coating. *Surf. Coat. Technol.* **2019**, *369*, 31–43. [\[CrossRef\]](#)

178. Kurzynowski, T.; Madeja, M.; Dziedzic, R.; Kobiela, K. The effect of EBM process parameters on porosity and microstructure of Ti-5Al-5Mo-5V-1Cr-1Fe alloy. *Scanning* **2019**, *2019*, 100–105. [[CrossRef](#)] [[PubMed](#)]
179. Burstein, A.H.; Reilly, D.T.; Martens, M. Aging of bone tissue: Mechanical properties. *J. Bone Jt. Surg.* **1976**, *58*, 82–86. [[CrossRef](#)]
180. Ding, M.; Dalstra, M.; Danielsen, C.C.; Kabel, J.; Hvid, I.; Linde, F. Age variations in the properties of human tibial trabecular bone. *J. Bone Jt. Surg.* **1997**, *79*, 995–1002. [[CrossRef](#)]
181. Krishna, B.V.; Xue, W.; Bose, S.; Bandyopadhyay, A. Engineered porous metals for implants. *JOM* **2008**, *60*, 45–48. [[CrossRef](#)]
182. Xue, W.; Krishna, B.V.; Bandyopadhyay, A.; Bose, S. Processing and biocompatibility evaluation of laser processed porous titanium. *Acta Biomater.* **2007**, *3*, 1007–1018. [[CrossRef](#)]
183. Bandyopadhyay, A.; Espana, F.; Balla, V.K.; Bose, S.; Ohgami, Y.; Davies, N.M. Influence of porosity on mechanical properties and in vivo response of Ti6Al4V implants. *Acta Biomater.* **2010**, *6*, 1640–1648. [[CrossRef](#)]
184. Kalita, D.; Rogal, Ł.; Bobrowski, P.; Durejko, T.; Czujko, T.; Antolak-Dudka, A.; Cesari, E.; Dutkiewicz, J. Superelastic behavior of Ti-Nb alloys obtained by the Laser Engineered Net Shaping (LENS) technique. *Materials* **2020**, *13*, 2827. [[CrossRef](#)]
185. Clark, D.; Whittaker, M.T.; Bache, M.R. Microstructural characterization of a prototype titanium alloy structure processed via direct laser deposition (DLD). *Metall. Mater. Trans. B* **2012**, *43*, 388–396. [[CrossRef](#)]
186. Yilmaz, O.; Ugla, A.A. Shaped metal deposition technique in additive manufacturing: A review. *Proc. Inst. Mech. Eng. Pt. B J. Eng. Manuf.* **2016**, *230*, 1781–1798. [[CrossRef](#)]
187. Childerhouse, T.; Jackson, M. Near net shape manufacture of titanium alloy components from powder and wire: A review of state-of-the-art process routes. *Metals* **2019**, *9*, 689. [[CrossRef](#)]
188. Weston, N.S.; Jackson, M. FAST-forge—A new cost-effective hybrid processing route for consolidating titanium powder into near net shape forged components. *J. Mater. Process. Technol.* **2017**, *243*, 335–346. [[CrossRef](#)]
189. Calvert, E.; Wynne, B.; Weston, N.; Tudball, A.; Jackson, M. Thermomechanical processing of a high strength metastable beta titanium alloy powder, consolidated using the low-cost FAST-forge process. *J. Mater. Process. Technol.* **2018**, *254*, 158–170. [[CrossRef](#)]
190. Chen, Q.; Thouas, G.A. Metallic implant biomaterials. *Mater. Sci. Eng. R Rep.* **2015**, *87*, 1–57. [[CrossRef](#)]
191. Nakano, T. Mechanical properties of metallic biomaterials. In *Metals for Biomedical Devices*; Elsevier: Amsterdam, The Netherlands, 2010; pp. 71–98.
192. Liu, Y.J.; Wang, H.L.; Li, S.J.; Wang, S.G.; Wang, W.J.; Hou, W.T.; Hao, Y.L.; Yang, R.; Zhang, L.C. Compressive and fatigue behavior of beta-type titanium porous structures fabricated by electron beam melting. *Acta Mater.* **2017**, *126*, 58–66. [[CrossRef](#)]
193. Kent, D.; Wang, G.; Dargusch, M. Effects of phase stability and processing on the mechanical properties of Ti-Nb based beta Ti alloys. *J. Mech. Behav. Biomed. Mater.* **2013**, *28*, 15–25. [[CrossRef](#)]
194. Niinomi, M.; Nakai, M. Titanium-based biomaterials for preventing stress shielding between implant devices and bone. *Int. J. Biomater.* **2011**, *2011*, 836587. [[CrossRef](#)]
195. Rabadia, C.D.; Liu, Y.J.; Zhao, C.H.; Wang, J.C.; Jawed, S.F.; Wang, L.Q.; Chen, L.Y.; Sun, H.; Zhang, L.C. Improved trade-off between strength and plasticity in titanium based metastable beta type Ti-Zr-Fe-Sn alloys. *Mater. Sci. Eng. A* **2019**, *766*, 138340. [[CrossRef](#)]
196. Laheurte, P.; Prima, F.; Eberhardt, A.; Gloriant, T.; Wary, M.; Patoor, E. Mechanical properties of low modulus beta titanium alloys designed from the electronic approach. *J. Mech. Behav. Biomed. Mater.* **2010**, *3*, 565–573. [[CrossRef](#)] [[PubMed](#)]
197. Bermingham, M.J.; McDonald, S.D.; Dargusch, M.S.; StJohn, D.H. Grain-refinement mechanisms in titanium alloys. *J. Mater. Res.* **2008**, *23*, 97–104. [[CrossRef](#)]
198. Dai, S.-J.; Wang, Y.; Chen, F.; Yu, X.-Q.; Zhang, Y.-F. Influence of Zr content on microstructure and mechanical properties of implant Ti-35Nb-4Sn-6Mo-xZr alloys. *Trans. Nonfer. Metall. Soc. China* **2013**, *23*, 1299–1303. [[CrossRef](#)]
199. Xu, Y.; Gao, J.; Huang, Y.; Rainforth, W.M. A low-cost metastable beta Ti alloy with high elastic admissible strain and enhanced ductility for orthopaedic application. *J. Alloys Compd.* **2020**, *835*, 155391. [[CrossRef](#)]
200. Liang, S.X.; Feng, X.J.; Yin, L.X.; Liu, X.Y.; Ma, M.Z.; Liu, R.P. Development of a new  $\beta$  Ti alloy with low modulus and favorable plasticity for implant material. *Mater. Sci. Eng. C* **2016**, *61*, 338–343. [[CrossRef](#)]



201. Coakley, J.; Isheim, D.; Radecka, A.; Dye, D.; Stone, H.J.; Seidman, D.N. Microstructural evolution in a superelastic metastable beta-Ti alloy. *Scr. Mater.* **2017**, *128*, 87–90. [\[CrossRef\]](#)
202. Kuroda, P.A.B.; Lourenço, M.L.; Correa, D.R.N.; Grandini, C.R. Thermomechanical treatments influence on the phase composition, microstructure, and selected mechanical properties of Ti–20Zr–Mo alloys system for biomedical applications. *J. Alloys Compd.* **2020**, *812*, 152108. [\[CrossRef\]](#)
203. Lee, S.H.; Todai, M.; Tane, M.; Hagihara, K.; Nakajima, H.; Nakano, T. Biocompatible low Young's modulus achieved by strong crystallographic elastic anisotropy in Ti–15Mo–5Zr–3Al alloy single crystal. *J. Mech. Behav. Biomed. Mater.* **2012**, *14*, 48–54. [\[CrossRef\]](#)
204. Pellizzari, M.; Jam, A.; Tschon, M.; Fini, M.; Lora, C.; Benedetti, M. A 3D-Printed Ultra-Low Young's Modulus  $\beta$ -Ti Alloy for Biomedical Applications. *Materials* **2020**, *13*, 2792. [\[CrossRef\]](#)
205. Lee, T.; Lee, S.; Kim, I.-S.; Moon, Y.H.; Kim, H.S.; Park, C.H. Breaking the limit of Young's modulus in low-cost Ti–Nb–Zr alloy for biomedical implant applications. *J. Alloys Compd.* **2020**, *828*, 154401. [\[CrossRef\]](#)
206. Rabadia, C.D.; Liu, Y.J.; Jawed, S.F.; Wang, L.; Li, Y.H.; Zhang, X.H.; Sercombe, T.B.; Sun, H.; Zhang, L.C. Improved deformation behavior in Ti–Zr–Fe–Mn alloys comprising the C14 type Laves and  $\beta$  phases. *Mater. Des.* **2018**, *160*, 1059–1070. [\[CrossRef\]](#)
207. Rabadia, C.D.; Liu, Y.J.; Jawed, S.F.; Wang, L.Q.; Sun, H.; Zhang, L.C. Deformation and toughness behavior of  $\beta$ -type titanium alloys comprising C15-type Laves phase. *Mater. Today Sustain.* **2020**, *9*, 100034. [\[CrossRef\]](#)
208. Chen, Y.; Zhang, J.; Dai, N.; Qin, P.; Attar, H.; Zhang, L.-C. Corrosion behaviour of selective laser melted Ti–TiB biocomposite in simulated body fluid. *Electrochim. Acta* **2017**, *232*, 89–97. [\[CrossRef\]](#)
209. Dai, N.; Zhang, L.-C.; Zhang, J.; Chen, Q.; Wu, M. Corrosion behavior of selective laser melted Ti–6Al–4V alloy in NaCl solution. *Corros. Sci.* **2016**, *102*, 484–489. [\[CrossRef\]](#)
210. Qin, P.; Liu, Y.; Sercombe, T.B.; Li, Y.; Zhang, C.; Cao, C.; Sun, H.; Zhang, L.-C. Improved corrosion resistance on selective laser melting produced Ti–5Cu alloy after heat treatment. *ACS Biomater. Sci. Eng.* **2018**, *4*, 2633–2642. [\[CrossRef\]](#)
211. Alves, A.P.R.; Santana, F.A.; Rosa, L.A.A.; Cursino, S.A.; Codaro, E.N. A study on corrosion resistance of the Ti–10Mo experimental alloy after different processing methods. *Mater. Sci. Eng. C* **2004**, *24*, 693–696. [\[CrossRef\]](#)
212. Qin, X.; Guo, X.; Lu, J.; Chen, L.; Qin, J.; Lu, W. Erosion-wear and intergranular corrosion resistance properties of AISI 304L austenitic stainless steel after low-temperature plasma nitriding. *J. Alloys Compd.* **2017**, *698*, 1094–1101. [\[CrossRef\]](#)
213. Zhang, L.C.; Jia, Z.; Lyu, F.; Liang, S.X.; Lu, J. A review of catalytic performance of metallic glasses in wastewater treatment: Recent progress and prospects. *Prog. Mater. Sci.* **2019**, *105*, 100576. [\[CrossRef\]](#)
214. Liang, S.X.; Jia, Z.; Liu, Y.J.; Zhang, W.; Wang, W.; Lu, J.; Zhang, L.C. Compelling rejuvenated catalytic performance in metallic glasses. *Adv. Mater.* **2018**, *30*, 1802764. [\[CrossRef\]](#)
215. Alves, V.A.; Reis, R.Q.; Santos, I.C.B.; Souza, D.G.; Gonçalves, T.D.F.; Pereira-da-Silva, M.A.; Rossi, A.; da Silva, L.A. In situ impedance spectroscopy study of the electrochemical corrosion of Ti and Ti–6Al–4V in simulated body fluid at 25 °C and 37 °C. *Corros. Sci.* **2009**, *51*, 2473–2482. [\[CrossRef\]](#)
216. Loch, J.; Łukaszczuk, A.; Vignal, V.; Krawiec, H. Corrosion behaviour of Ti6Al4V and TiMo10Zr4 alloys in the Ringer's solution: Effect of pH and plastic strain. *Solid State Phenom.* **2015**, *227*, 435–438. [\[CrossRef\]](#)
217. Simsek, I.; Ozyurek, D. Investigation of the wear and corrosion behaviors of Ti5Al2.5Fe and Ti6Al4V alloys produced by mechanical alloying method in simulated body fluid environment. *Mater. Sci. Eng. C* **2019**, *94*, 357–363. [\[CrossRef\]](#)
218. Chui, P.; Jing, R.; Zhang, F.; Li, J.; Feng, T. Mechanical properties and corrosion behavior of  $\beta$ -type Ti–Zr–Nb–Mo alloys for biomedical application. *J. Alloys Compd.* **2020**, *842*, 155693. [\[CrossRef\]](#)
219. Zareidoost, A.; Yousefpour, M. A study on the mechanical properties and corrosion behavior of the new as-cast TZNT alloys for biomedical applications. *Mater. Sci. Eng. C* **2020**, *110*, 110725. [\[CrossRef\]](#) [\[PubMed\]](#)
220. Lin, J.; Ozan, S.; Munir, K.; Wang, K.; Tong, X.; Li, Y.; Li, G.; Wen, C. Effects of solution treatment and aging on the microstructure, mechanical properties, and corrosion resistance of a  $\beta$  type Ti–Ta–Hf–Zr alloy. *RSC Adv.* **2017**, *7*, 12309–12317. [\[CrossRef\]](#)
221. Dai, N.; Zhang, L.-C.; Zhang, J.; Zhang, X.; Ni, Q.; Chen, Y.; Wu, M.; Yang, C. Distinction in corrosion resistance of selective laser melted Ti–6Al–4V alloy on different planes. *Corros. Sci.* **2016**, *111*, 703–710. [\[CrossRef\]](#)



222. Atapour, M.; Pilchak, A.L.; Frankel, G.S.; Williams, J.C. Corrosion behavior of  $\beta$  titanium alloys for biomedical applications. *Mater. Sci. Eng. C* **2011**, *31*, 885–891. [\[CrossRef\]](#)
223. Williams, W.L. Development of structural titanium alloys for marine applications. *Ocean Eng.* **1969**, *1*, 375–383. [\[CrossRef\]](#)
224. Lu, H.-B.; Poh, C.-K.; Zhang, L.C.; Guo, Z.P.; Yu, X.B.; Liu, H.-K. Dehydrogenation characteristics of Ti-and Ni/Ti-catalyzed Mg hydrides. *J. Alloys Compd.* **2009**, *481*, 152–155. [\[CrossRef\]](#)
225. Dai, N.; Zhang, J.; Chen, Y.; Zhang, L.-C. Heat treatment degrading the corrosion resistance of selective laser melted Ti-6Al-4V alloy. *J. Electrochem. Soc.* **2017**, *164*, C428–C434. [\[CrossRef\]](#)
226. Zhang, B.; Wang, J.; Wu, B.; Guo, X.W.; Wang, Y.J.; Chen, D.; Zhang, Y.C.; Du, K.; Oguzie, E.E.; Ma, X.L. Unmasking chloride attack on the passive film of metals. *Nat. Commun.* **2018**, *9*, 2559. [\[CrossRef\]](#) [\[PubMed\]](#)
227. Lu, H.; Zhang, L.; Gebert, A.; Schultz, L. Pitting corrosion of Cu–Zr metallic glasses in hydrochloric acid solutions. *J. Alloys Compd.* **2008**, *462*, 60–67. [\[CrossRef\]](#)
228. Zhang, L.; Chen, L.-Y.; Zhao, C.; Liu, Y.; Zhang, L.-C. Calculation of oxygen diffusion coefficients in oxide films formed on low-temperature annealed Zr alloys and their related corrosion behavior. *Metals* **2019**, *9*, 850. [\[CrossRef\]](#)
229. Schutz, R.W. Environmental behavior of beta titanium alloys. *JOM* **1994**, *46*, 24–29. [\[CrossRef\]](#)
230. McMahon, R.E.; Ma, J.; Verkhovurov, S.V.; Munoz-Pinto, D.; Karaman, I.; Rubitschek, F.; Maier, H.J.; Hahn, M.S. A comparative study of the cytotoxicity and corrosion resistance of nickel-titanium and titanium-niobium shape memory alloys. *Acta Biomater.* **2012**, *8*, 2863–2870. [\[CrossRef\]](#)
231. Xue, P.; Li, Y.; Li, K.; Zhang, D.; Zhou, C. Superelasticity, corrosion resistance and biocompatibility of the Ti-19Zr-10Nb-1Fe alloy. *Mater. Sci. Eng. C* **2015**, *50*, 179–186. [\[CrossRef\]](#)
232. Takematsu, E.; Katsumata, K.-i.; Okada, K.; Niinomi, M.; Matsushita, N. Bioactive surface modification of Ti-29Nb-13Ta-4.6 Zr alloy through alkali solution treatments. *Mater. Sci. Eng. C* **2016**, *62*, 662–667. [\[CrossRef\]](#)
233. Dikici, B.; Niinomi, M.; Topuz, M.; Koc, S.G.; Nakai, M. Synthesis of biphasic calcium phosphate (BCP) coatings on  $\beta$ -type titanium alloys reinforced with rutile-TiO<sub>2</sub> compounds: Adhesion resistance and in-vitro corrosion. *J. Sol-Gel Sci. Technol.* **2018**, *87*, 713–724. [\[CrossRef\]](#)
234. Morra, M.; Cassinelli, C.; Cascardo, G.; Bollati, D.; Baena, R.R. Gene expression of markers of osteogenic differentiation of human mesenchymal cells on collagen I-modified microrough titanium surfaces. *J. Biomed. Mater. Res. A* **2011**, *96*, 449–455. [\[CrossRef\]](#)
235. Hoene, A.; Walschus, U.; Patrzyk, M.; Finke, B.; Lucke, S.; Nebe, B.; Schroeder, K.; Ohl, A.; Schlosser, M. In vivo investigation of the inflammatory response against allylamine plasma polymer coated titanium implants in a rat model. *Acta Biomater.* **2010**, *6*, 676–683. [\[CrossRef\]](#)



© 2020 by the authors. Licensee MDPI, Basel, Switzerland. This article is an open access article distributed under the terms and conditions of the Creative Commons Attribution (CC BY) license (<http://creativecommons.org/licenses/by/4.0/>).